3D-1D coupling on non conforming meshes via a three-field optimization based domain decomposition

3D-1D coupling on non conforming meshes via a three-field optimization based domain decomposition

Stefano Berrone[a], Denise Grappein[a], Stefano Scialò[a,*]

[a] *Dipartimento di Scienze Matematiche, Politecnico di Torino, Corso Duca degli Abruzzi 24, 10129 Torino, Italy. Member of INdAM research group GNCS.*

Abstract

A new numerical approach is proposed for the simulation of coupled three-dimensional and one-dimensional elliptic equations (3D-1D coupling) arising from dimensionality reduction of 3D-3D problems with thin inclusions. The method is based on a well posed mathematical formulation and results in a numerical scheme with high flexibility in handling geometrical complexities. This is achieved by means of a three-field approach to split the 1D problems from the bulk 3D problem, and then resorting to the minimization of a properly designed functional to impose matching conditions at the interfaces. Thanks to the structure of the functional, the method allows the use of independent meshes for the various subdomains.

Keywords: 3D-1D coupling, three-field, domain-decomposition, non conforming mesh, optimization methods for elliptic problems
2010 MSC: 65N30, 65N50, 68U20, 86-08

1. Introduction

This work presents a new numerical approach to manage the coupling of three-dimensional and one-dimensional elliptic equations (3D-1D coupling). This kind of problems emerges, for example, in the numerical treatment of domains with small tubular inclusions: in these cases, indeed, it might be computationally convenient to approximate the small inclusions by one-dimensional (1D) manifolds, in order to avoid the building of a three-dimensional grid within the inclusion. Clearly this topological reduction can be a viable approach only if one-dimensional modeling assumptions can be applied to the problem at hand. Examples of application are: capillary networks exchanging flux with the surrounding tissue [1, 2], the interaction of plant roots with the soil [3, 4], a system of wells in geological applications [5, 6, 7], or the modeling of fiber-reinforced materials [8, 9].

*Corresponding author
Email addresses: stefano.berrone@polito.it (Stefano Berrone), denise.grappein@polito.it (Denise Grappein), stefano.scialo@polito.it (Stefano Scialò)

The definition of coupling conditions between a three-dimensional (3D) and a 1D problem is not straightforward, as no bounded trace operator is defined in standard functional spaces on manifolds with a dimensionality gap higher than one. This problem was recently studied in [10, 11], where suitably weighted Sobolev spaces were introduced and a bounded trace operator from the 3D space to the 1D space was defined, thus allowing to formulate a well posed coupled problem, also resorting to the results in [12]. In [13] regularizing techniques are proposed for singular terms. Three dimensional problems with singular sources defined on lines are also studied in [14], where the nature of the irregularity is analyzed and a method based on the splitting of the solution in a low regularity part plus a regular correction is proposed. Problems with a source term on manifolds with high dimensionality gaps are also studied in [15], where a lifting technique of the irregular datum is used to reduce the dimensionality gap. In [16], regularized singular source terms are introduced and scaling factors are used to select the scale at which such source terms are activated, independently from the mesh resolution. In the method proposed in [17], instead, the singular source terms arising from 3D-1D coupled problems are approximated in a neighbourhood of the inclusions by custom kernel functions. In [18] a 3D-1D coupled approach is derived starting from the fully 3D-3D coupled problem and applying a topological model reduction through the definition of proper averaging operators. Mixed dimensional PDEs on 3D-1D domains are also addressed in [19], using Lagrange multipliers to enforce the coupling. A stabilization is required to ensure well posedness of the discrete problem for some choices of the space of multipliers.

In the present work a new numerical approach to this problem is proposed, starting from modeling assumptions similar to those proposed in [18]. A reduced 3D-1D model approximating the original equi-dimensional 3D-3D problem is here obtained by introducing proper assumptions on the solution inside the small inclusions and by defining suitable subspaces of the Sobolev spaces typically employed in the variational formulation of partial differential equations. In this respect, the proposed approach differs from the others available in literature, and in particular from the approach in [18]. Indeed, here a continuous well posed 3D-1D coupled problem is obtained by assuming that the solution is constant in the cross sectional area of the inclusions and introducing suitable extensions and trace operators. Thanks to this, the problem is treated, in practice, as a 3D-1D reduced problem, but it can still be written as an equi-dimensional problem, thus skipping the difficulties related to the 3D-1D coupling. The problems in the bulk 3D domain and in the small inclusions are splitted resorting to a three-field based domain decomposition method, originally formulated in [20] and already applied for domain decomposition in networks of fractures [21]. Suitable matching conditions are then enforced at the interface to recover the solution on the whole domain. Here pressure continuity and flux conservation constraints are assumed at the interfaces. This kind of interface conditions are also considered in the approaches proposed in [19] and [8], for example, and are relevant for applications, as, e.g., the simulation of *leaky* vessels in angiogenesis [22], thin membranes [23], or fiber-reinforced materials [8]. The advantages

of the three-field based approach with respect to other domain decomposition methods lie in the possibility of defining stable locally conservative numerical schemes on non conforming meshes [21], on the direct computation of the interface variables, and on the definition of a well posed discrete problem on non conforming meshes independently of the choice of the space of the discrete variables. Matching conditions at the interfaces are enforced by means of a PDE constrained numerical scheme, already proposed for simulation of the flow in poro-fractured media [24, 25, 26] and here proposed for 3D-1D coupling. The method is based on the minimization of a cost functional expressing the error in the fulfillment of interface conditions, constrained by constitutive laws on the various subdomains. The advantages of such an approach lie in the possibility of enforcing continuity and flux balance at the interfaces using completely independent meshes on the sub-domains. This provides to the scheme an extreme flexibility and robustness to geometrical complexities, which are critical features for the applicability to real problems, where the nearly one dimensional inclusions might form complex networks, possibly generated from random parameters [27, 28]. Exploiting the properties of the functional spaces chosen for the solution, the functional can be reduced to the centrelines of the tubular inclusions and used to control the continuity of the solution, whereas flux conservation is strongly enforced thanks to the three-field formulation. High jumps of the coefficients across the interfaces are also permitted by the proposed approach.

The manuscript is organized as follows: in Section 2 notation is introduced and the strong formulation of the 3D-3D problem is presented, along with the hypotheses allowing its reduction to a 3D-1D problem. In Section 3 the weak formulation of the 3D-1D coupled problem is worked out, while in Section 4 the problem is re-written into a PDE-constrained optimization formulation. The corresponding discrete approach is discussed in Section 6. Finally, in Section 7, some numerical examples are described.

2. Notation and problem formulation

Let us here briefly recall the basic formulation of the problem of interest in a simplified setting, the ideas here proposed being easily extendable to more general cases. We refer to [18] for a broader presentation of the problem. Let us consider a convex domain $\Omega \subset \mathbb{R}^3$ in which a generalized cylinder $\Sigma \subset \mathbb{R}^3$ is embedded. The centreline of this cylinder is denoted by $\Lambda = \{\boldsymbol{\lambda}(s), s \in (0, S)\}$, where $\boldsymbol{\lambda}(s)$ is here assumed, for simplicity, to be a rectilinear segment in the three-dimensional space. The symbol $\Sigma(s)$ denotes the transversal section of the cylinder at $s \in [0, S]$. We assume that each section, whose boundary is denoted by $\Gamma(s)$, has an elliptic shape, denoting by R the maximum axes length of the ellipses as s ranges in the interval $[0, S]$. The lateral surface of Σ is $\Gamma = \{\Gamma(s),\ s \in [0, S]\}$, while $\Sigma_0 = \Sigma(0)$ and $\Sigma_S = \Sigma(S)$ are the two extreme sections. The portion of the domain that does not include the cylinder is denoted by $D = \Omega \setminus \Sigma$, with boundary $\partial D = \partial\Omega \cup \{\Gamma \cup \Sigma_0 \cup \Sigma_S\}$, where $\partial\Omega$ is the boundary of Ω. We refer to ∂D^e as the external boundary of D, coinciding with

$\partial\Omega$ when the extreme sections of Σ are inside Ω. In case Σ_0 and Σ_S lie on the boundary $\partial\Omega$ we define $\partial D^e = \partial\Omega \setminus \{\Sigma_0 \cup \Sigma_S\}$.

Let us consider, in Ω, a diffusion problem, with unknown pressures u in D and $\tilde{u}$ in Σ:

3D-problem on D:

$$-\nabla \cdot (K\nabla u) = f \quad \text{in } D \quad (1)$$
$$u = 0 \quad \text{on } \partial D^e \quad (2)$$
$$u_{|\Gamma} = \psi \quad \text{on } \Gamma \quad (3)$$
$$K\nabla u \cdot \boldsymbol{n} = \phi \quad \text{on } \Gamma \quad (4)$$

3D-problem on Σ:

$$-\nabla \cdot (\tilde{K}\nabla \tilde{u}) = g \quad \text{in } \Sigma \quad (5)$$
$$\tilde{u} = 0 \quad \text{on } \Sigma_0 \cup \Sigma_S \quad (6)$$
$$\tilde{u}_{|\Gamma} = \psi \quad \text{on } \Gamma \quad (7)$$
$$\tilde{K}\nabla \tilde{u} \cdot \tilde{\boldsymbol{n}} = -\phi \quad \text{on } \Gamma \quad (8)$$

Vectors $\boldsymbol{n}$ and $\tilde{\boldsymbol{n}}$ are the outward pointing unit normal vectors to Γ, respectively for D and Σ, such that $\tilde{\boldsymbol{n}} = -\boldsymbol{n}$, K and $\tilde{K}$ are positive scalars, and f and g are source terms. The symbol ψ denotes the unknown unique value of the pressure on the interface Γ while ϕ is the unknown flux through Γ, entering in D. For the sake of simplicity we suppose here that the extreme sections Σ_0 and Σ_S lie on $\partial\Omega$, and we consider homogeneous Dirichlet boundary conditions on both of them and on ∂D^e, the extension to more general cases being straightforward. Equations (3)-(4) and (7)-(8) enforce pressure continuity and flux conservation constraints on the lateral surface Γ of the cylinder, thus allowing us to couple the two problems. We remark that different coupling conditions could be considered, as the ones proposed in [18].

If the cross-section-size R of the cylinder Σ becomes much smaller than both the longitudinal length L and the characteristic dimension of Ω, a model can be introduced in order to reduce the computational cost of simulations. The key point is that, as $R \ll L$, it is possible to assume that the variations of $\tilde{u}$ on the transversal sections of the cylinder are negligible, i.e., in cylindrical coordinates,

$$\tilde{u}(r, \theta, s) = \hat{u}(s) \quad \forall r \in [0, R],\ \forall \theta \in [0, 2\pi). \quad (9)$$

This allows us to simplify problem (5)-(6) reducing it to a 1D problem defined on the cylinder's centerline Λ as

$$-\frac{d}{ds}\left(\tilde{K}|\Sigma(s)|\frac{d\hat{u}}{ds}\right) = \tilde{g} \qquad \text{for } s \in (0, S) \quad (10)$$
$$\hat{u}(0) = \hat{u}(S) = 0, \quad (11)$$

where the new forcing term $\tilde{g}$ now accounts for the original volumetric source g and for the incoming flux from the boundary Γ of the equi-dimensional problem. Details of this geometrical reduction are provided in the next session. The clear advantage of the reduced problem (10)-(11) is that solving a problem defined on a segment instead of a problem defined on a small cylinder is computationally much cheaper, and avoids the necessity of a 3D-1D trace operator.

In the next section an original formulation of the coupled 3D-1D problem is derived, starting from a variational formulation of the fully dimensional 3D-3D problem (1)-(2) and (5)-(6), and defining the proper functional spaces and operators required to reduce this formulation to a well posed 3D-1D coupling.

3. Variational formulation

In this section we will adopt the following notation:

$$H_0^1(D) = \left\{v \in H^1(D) : v_{|_{\partial D^e}} = 0\right\}$$
$$H_0^1(\Sigma) = \left\{v \in H^1(\Sigma) : v_{|_{\Sigma_0}} = v_{|_{\Sigma_S}} = 0\right\}$$
$$H_0^1(\Lambda) = \left\{v \in H^1(\Lambda) : v(0) = v(S) = 0\right\}$$

and we will suppose that $\partial D^e = \partial\Omega \setminus \{\Sigma_0 \cup \Sigma_S\}$, i.e. the extreme sections of the cylinder lie on $\partial\Omega$. As aforementioned this assumption is introduced for the sake of simplicity, the formulation being extendable to more general cases. Let us define a trace operator

$$\gamma_{_\Gamma} : H^1(D) \cup H^1(\Sigma) \to H^{\frac{1}{2}}(\Gamma), \text{ such that } \gamma_{_\Gamma} v = v_{|_\Gamma} \ \forall v \in H^1(D) \cup H^1(\Sigma) \quad (12)$$

and two extension operators

$$\mathcal{E}_{_\Sigma} : H^1(\Lambda) \to H^1(\Sigma) \ \text{ and } \ \mathcal{E}_{_\Gamma} : H^1(\Lambda) \to H^{\frac{1}{2}}(\Gamma)$$

defined such that, given $\hat{v} \in H_0^1(\Lambda)$, $\mathcal{E}_{_\Sigma}(\hat{v})$ is the uniform extension of the pointwise value $\hat{v}(s)$, $s \in [0, S]$, to the cross section $\Sigma(s)$ of the cylinder and $\mathcal{E}_{_\Gamma}(\hat{v})$ the uniform extension of $\hat{v}$ to the boundary $\Gamma(s)$ of the cross section, i.e.

$$\mathcal{E}_{_\Sigma}\hat{v}(\boldsymbol{x}) = \hat{v}(s) \ \forall \boldsymbol{x} \in \Sigma(s) \quad \text{and} \quad \mathcal{E}_{_\Gamma}\hat{v}(\boldsymbol{x}) = \hat{v}(s) \ \forall \boldsymbol{x} \in \Gamma(s).$$

Let us observe that $\mathcal{E}_{_\Gamma} = \gamma_{_\Gamma} \circ \mathcal{E}_{_\Sigma}$. Setting $\hat{V} = H_0^1(\Lambda)$, let us further consider the spaces:

$$\widetilde{V} = \{v \in H_0^1(\Sigma) : v = \mathcal{E}_{_\Sigma}\hat{v}, \ \hat{v} \in \hat{V}\},$$
$$\mathcal{H}^{\Gamma} = \{v \in H^{\frac{1}{2}}(\Gamma) : v = \mathcal{E}_{_\Gamma}\hat{v}, \ \hat{v} \in \hat{V}\},$$
$$V_D = \left\{v \in H_0^1(D) : \gamma_{_\Gamma} v \in \mathcal{H}^{\Gamma}\right\}.$$

such that $\widetilde{V} \subset H_0^1(\Sigma)$ contains functions that are extensions to the whole Σ of functions in $\hat{V}$, $\mathcal{H}^{\Gamma} \subset H^{\frac{1}{2}}(\Gamma)$ contains functions that are extensions to Γ of functions in $\hat{V}$, and $V_D \subset H_0^1(D)$ only contains functions whose trace on Γ is a function of $\mathcal{H}^{\Gamma}$. Denoting by $(\cdot,\cdot)_\star$ the L^2-scalar product on a generic domain $\star$, and by X' the dual of a generic space X, the variational problem arising from the coupling of (1)-(2) and (5)-(6) through the continuity constraint can be written as: *find* $(u, \tilde{u}) \in V_D \times \widetilde{V}$ *such that*

$$(K\nabla u, \nabla v)_D + (\tilde{K}\nabla\tilde{u}, \nabla\tilde{v})_\Sigma = (f, v)_D + (g, \tilde{v})_\Sigma \qquad \forall (v, \tilde{v}) \in V_D \times \widetilde{V} \quad (13)$$
$$\langle \gamma_{_\Gamma} u - \gamma_{_\Gamma}\tilde{u}, \eta\rangle_{\mathcal{H}^{\Gamma}, \mathcal{H}^{\Gamma\prime}} = 0, \qquad \forall \eta \in \mathcal{H}^{\Gamma\prime} \quad (14)$$

Remark 1. *Let us consider the space* $\mathbb{V} = \left\{(v, \tilde{v}) \in V_D \times \widetilde{V} : \gamma_{_\Gamma} v = \gamma_{_\Gamma}\tilde{v}\right\}$. *Then, problem (13)-(14) is equivalent to: find* $(u, \tilde{u}) \in \mathbb{V}$ *such that*

$$(K\nabla u, \nabla v)_D + (\tilde{K}\nabla\tilde{u}, \nabla\tilde{v})_\Sigma = (f, v)_D + (g, \tilde{v})_\Sigma \ \ \forall (v, \tilde{v}) \in \mathbb{V}$$

The well-posedness of the problem easily follows from Lax-Milgram theorem, considering $||\cdot||_{\mathbb{V}} = ||\cdot||_{H^1(D)} + ||\cdot||_{H^1(\Sigma)}$

Equation (13) can be split into two coupled equations introducing the unknown flux ϕ through Γ, obtaining thus

$$(K\nabla u, \nabla v)_D - \langle \phi, \gamma_{\Gamma} v \rangle_{\mathcal{H}^{\Gamma'}, \mathcal{H}^{\Gamma}} = (f, v)_D \qquad \forall v \in V_D,\ \phi \in \mathcal{H}^{\Gamma'} \tag{15}$$

$$(\tilde{K}\nabla \tilde{u}, \nabla \tilde{v})_{\Sigma} + \langle \phi, \gamma_{\Gamma} \tilde{v} \rangle_{\mathcal{H}^{\Gamma'}, \mathcal{H}^{\Gamma}} = (g, \tilde{v})_{\Sigma} \qquad \forall \tilde{v} \in \widetilde{V},\ \phi \in \mathcal{H}^{\Gamma'} \tag{16}$$

Moreover, the continuity condition (14) can be rewritten introducing a new variable $\psi \in \mathcal{H}^{\Gamma}$ as:

$$\langle \gamma_{\Gamma} u - \psi, \eta \rangle_{\mathcal{H}^{\Gamma}, \mathcal{H}^{\Gamma'}} = 0 \qquad \forall \eta \in \mathcal{H}^{\Gamma'}, \psi \in \mathcal{H}^{\Gamma} \tag{17}$$

$$\langle \gamma_{\Gamma} \tilde{u} - \psi, \eta \rangle_{\mathcal{H}^{\Gamma}, \mathcal{H}^{\Gamma'}} = 0 \qquad \forall \eta \in \mathcal{H}^{\Gamma'}, \psi \in \mathcal{H}^{\Gamma}. \tag{18}$$

The set of equations (15), (16), (17) and (18) represent an application of the three-field formulation presented in [20] and similarly applied in [21].

Thanks to the assumptions on the introduced functional spaces, this problem can be reduced to a 3D-1D coupled problem without encountering the aforementioned issues in the definition of a trace operator. In fact we only need to use the trace operator $\gamma_{\Gamma}(\cdot)$, which is well-posed as defined from a three-dimensional manifold to a two dimensional one. Let us observe that

$$\langle \phi, \gamma_{\Gamma} v \rangle_{\mathcal{H}^{\Gamma'}, \mathcal{H}^{\Gamma}} = \int_{\Gamma} \phi\ \gamma_{\Gamma} v\ d\Gamma = \int_0^S \Big(\int_{\Gamma(s)} \phi\ \gamma_{\Gamma} v\ dl \Big) ds \quad \forall v \in V_D$$

and let us denote by $\overline{\phi}(s)$ the mean value of ϕ on the border $\Gamma(s)$ of each section. As $v \in V_D$ we know that $\gamma_{\Gamma} v \in \mathcal{H}^{\Gamma}$, i.e. $\exists \check{v} \in \hat{V} : \gamma_{\Gamma} v = \mathcal{E}_{\Gamma} \check{v}$. Thus $\int_{\Gamma(s)} \gamma_{\Gamma} v\ dl = |\Gamma(s)| \check{v}(s)$ and

$$\int_0^S \Big(\int_{\Gamma(s)} \phi\ \gamma_{\Gamma} v\ dl \Big) ds = \int_0^S |\Gamma(s)| \overline{\phi}(s) \check{v}(s)\ ds = \left\langle |\Gamma| \overline{\phi}, \check{v} \right\rangle_{\hat{V}', \hat{V}},$$

where $|\Gamma(s)|$ is the section perimeter size at $s \in [0, S]$. The same holds if we consider $\langle \phi, \gamma_{\Gamma} \tilde{v} \rangle_{\mathcal{H}^{\Gamma'}, \mathcal{H}^{\Gamma}}$. As $\tilde{v} \in \widetilde{V}$ we know that $\exists \hat{v} \in \hat{V} : \tilde{v} = \mathcal{E}_{\Sigma} \hat{v}$ and consequently $\gamma_{\Gamma} \tilde{v} = \gamma_{\Gamma} \mathcal{E}_{\Sigma} \tilde{v} = \mathcal{E}_{\Gamma} \hat{v}$, so that

$$\langle \phi, \gamma_{\Gamma} \tilde{v} \rangle_{\mathcal{H}^{\Gamma'}, \mathcal{H}^{\Gamma}} = \left\langle |\Gamma| \overline{\phi}, \hat{v}(s) \right\rangle_{\hat{V}', \hat{V}}.$$

Similarly, $\forall \eta \in \mathcal{H}^{\Gamma'}$ and $\forall \rho : \rho = \mathcal{E}_{\Gamma} \hat{\rho}$ with $\hat{\rho} \in \hat{V}$, we can write

$$\langle \rho, \eta \rangle_{\mathcal{H}^{\Gamma}, \mathcal{H}^{\Gamma'}} = \int_0^S \Big(\int_{\Gamma(s)} \rho \eta dl \Big) ds = \int_0^S |\Gamma(s)| \hat{\rho}(s) \overline{\eta}(s) ds = \langle \hat{\rho}, |\Gamma| \overline{\eta} \rangle_{\hat{V}, \hat{V}'} \tag{19}$$

where we have used $\int_{\Gamma(s)} \rho\ dl = |\Gamma(s)| \hat{\rho}$ and $\overline{\eta}(s)$ is the mean value of η on the border $\Gamma(s)$ of each section. Exploiting (19) we can rewrite conditions (17) and

(18) as

$$\langle \gamma_\Gamma u - \psi, \eta \rangle_{\mathcal{H}^\Gamma, \mathcal{H}^{\Gamma\prime}} = \left\langle |\Gamma|(\check{u} - \hat{\psi}), \overline{\eta} \right\rangle_{\hat{V}, \hat{V}'} = 0$$
$$\langle \gamma_\Gamma \tilde{u} - \psi, \eta \rangle_{\mathcal{H}^\Gamma, \mathcal{H}^{\Gamma\prime}} = \left\langle |\Gamma|(\hat{u} - \hat{\psi}), \overline{\eta} \right\rangle_{\hat{V}, \hat{V}'} = 0$$

where $\check{u}, \hat{\psi} \in \hat{V}$ are such that $\gamma_\Gamma u = \mathcal{E}_\Gamma \check{u}$, $\psi = \mathcal{E}_\Gamma \hat{\psi}$ and $\gamma_\Gamma \tilde{u} = \gamma_\Gamma \mathcal{E}_\Sigma \tilde{u} = \mathcal{E}_\Gamma \hat{u}$, as $\tilde{u} \in \widetilde{V}$. Finally let us observe that

$$(\tilde{K} \nabla \tilde{u}, \nabla \tilde{v})_\Sigma = \int_\Sigma \tilde{K} \nabla \tilde{u} \nabla \tilde{v} \, d\sigma = \int_0^S \tilde{K} |\Sigma(s)| \frac{d\hat{u}}{ds} \frac{d\hat{v}}{ds} \, ds$$

where $\hat{u}, \hat{v} \in \hat{V}$ are such that $\tilde{u} = \mathcal{E}_\Sigma \hat{u}$, $\tilde{v} = \mathcal{E}_\Sigma \hat{v}$ and $|\Sigma(s)|$ is the section area at $s \in [0, S]$. Problem (15)-(18) can now be rewritten as a reduced 3D-1D coupled problem: *Find* $(u, \hat{u}) \in V_D \times \hat{V}$, $\overline{\phi} \in \hat{V}'$ *and* $\hat{\psi} \in \hat{V}$ *such that:*

$$(\boldsymbol{K} \nabla u, \nabla v)_D - \left\langle |\Gamma| \overline{\phi}, \check{v} \right\rangle_{\hat{V}', \hat{V}} = (f, v)_D \quad \forall v \in V_D, \check{v} \in \hat{V} : \gamma_\Gamma v = \mathcal{E}_\Gamma \check{v} \tag{20}$$

$$\left(\tilde{K} |\Sigma| \frac{d\hat{u}}{ds}, \frac{d\hat{v}}{ds} \right)_\Lambda + \left\langle |\Gamma| \overline{\phi}, \hat{v} \right\rangle_{\hat{V}', \hat{V}} = (|\Sigma| \overline{\overline{g}}, \hat{v})_\Lambda \quad \forall \hat{v} \in \hat{V} \tag{21}$$

$$\left\langle |\Gamma|(\check{u} - \hat{\psi}), \overline{\eta} \right\rangle_{\hat{V}', \hat{V}} = 0 \qquad \gamma_\Gamma u = \mathcal{E}_\Gamma \check{u}, \ \forall \overline{\eta} \in \hat{V}' \tag{22}$$

$$\left\langle |\Gamma|(\hat{u} - \hat{\psi}), \overline{\eta} \right\rangle_{\hat{V}', \hat{V}} = 0 \qquad \forall \overline{\eta} \in \hat{V}' \tag{23}$$

with $\overline{\overline{g}}(s) = \frac{1}{|\Sigma(s)|} \int_{\Sigma(s)} g \, d\sigma$, being g sufficiently regular.

Remark 2. *Even if we started from the same modeling assumptions as in [18], the formulation of the problem here proposed is different, for the choice of the functional spaces of the solution. Indeed, here we assume that the solution is constant on the cross-sections of the inclusion, and this regularity assumption is actually used to allow for the dimensional reduction.*

4. PDE-constrained optimization problem

The fulfillment of conditions (22) and (23) can be obtained through the minimization of a cost functional. Since we want to formulate independent problems on the various sub-domains, in order to guarantee the well posedness of each problem independently from the imposed boundary conditions, we modify equations (20)-(21) as follows:

$$(\boldsymbol{K} \nabla u, \nabla v)_D + \alpha (|\Gamma| \check{u}, \check{v})_\Lambda - \left\langle |\Gamma| \overline{\phi}, \check{v} \right\rangle_{\hat{V}', \hat{V}} = (f, v)_D + \alpha (|\Gamma| \hat{\psi}, \check{v})_\Lambda \quad \forall v \in V_D, \ \check{v} \in \hat{V} : \gamma_\Gamma v = \mathcal{E}_\Gamma \check{v}, \tag{24}$$

$$\left(\tilde{K} |\Sigma| \frac{d\hat{u}}{ds}, \frac{d\hat{v}}{ds} \right)_\Lambda + \hat{\alpha} (|\Gamma| \hat{u}, \hat{v})_\Lambda + \left\langle |\Gamma| \overline{\phi}, \hat{v} \right\rangle_{\hat{V}', \hat{V}} = (|\Sigma| \overline{\overline{g}}, \hat{v})_\Lambda + \hat{\alpha} (|\Gamma| \hat{\psi}, \hat{v})_\Lambda \quad \forall \hat{v} \in \hat{V}. \tag{25}$$

with $\alpha, \hat{\alpha} > 0$ being arbitrary parameters. Let us now define the following functional

$$\begin{aligned} J(\overline{\phi}, \hat{\psi}) &= \frac{1}{2}\Big(||\gamma_{\Gamma} u(\overline{\phi}, \hat{\psi}) - \psi||^2_{\mathcal{H}^{\Gamma}} + ||\gamma_{\Gamma} \tilde{u}(\overline{\phi}, \hat{\psi}) - \psi||^2_{\mathcal{H}^{\Gamma}} \Big) \\ &= \frac{1}{2}\Big(||\gamma_{\Gamma} u(\overline{\phi}, \hat{\psi}) - \mathcal{E}_{\Gamma}\hat{\psi}||^2_{\mathcal{H}^{\Gamma}} + ||\gamma_{\Gamma} \mathcal{E}_{\Sigma} \hat{u}(\overline{\phi}, \hat{\psi}) - \mathcal{E}_{\Gamma}\hat{\psi}||^2_{\mathcal{H}^{\Gamma}} \Big) \end{aligned} \quad (26)$$

to be minimized constrained by (24) and (25). In order to rewrite the PDE-constrained optimization problem in a compact form, we consider the linear operators $A : V_D \to V_D'$, $\widehat{A} : \hat{V} \to \hat{V}'$, $B : \hat{V}' \to V_D'$, $\widehat{B} : \hat{V}' \to \hat{V}'$, $C : \hat{V} \to V_D'$ and $\widehat{C} : \hat{V} \to \hat{V}'$ such that:

$$\langle Au, v\rangle_{V_D', V_D} = (\boldsymbol{K}\nabla u, \nabla v)_D + \alpha(|\Gamma| \check{u}, \check{v})_{\Lambda} \quad v \in V_D,\ \check{v} \in \hat{V} : \gamma_{\Gamma} v = \mathcal{E}_{\Gamma}\check{v} \quad (27)$$

$$\Big\langle \widehat{A}\hat{u}, \hat{v} \Big\rangle_{\hat{V}', \hat{V}} = \Big(\tilde{K}|\Sigma| \frac{d\hat{u}}{ds}, \frac{d\hat{v}}{ds} \Big)_{\Lambda} + \hat{\alpha}(|\Gamma|\hat{u}, \hat{v})_{\Lambda} \qquad \hat{v} \in \hat{V} \quad (28)$$

$$\big\langle B\overline{\phi}, v \big\rangle_{V_D', V_D} = \big\langle |\Gamma|\overline{\phi}, \check{v} \big\rangle_{\hat{V}', \hat{V}} \qquad v \in V_D,\ \check{v} \in \hat{V} : \gamma_{\Gamma} v = \mathcal{E}_{\Gamma}\check{v} \quad (29)$$

$$\Big\langle \widehat{B}\overline{\phi}, \hat{v} \Big\rangle_{\hat{V}', \hat{V}} = \big\langle |\Gamma|\overline{\phi}, \hat{v} \big\rangle_{\hat{V}', \hat{V}} \qquad \hat{v} \in \hat{V} \quad (30)$$

$$\Big\langle C\hat{\psi}, v \Big\rangle_{V_D', V_D} = \alpha(|\Gamma|\hat{\psi}, \check{v})_{\Lambda} \qquad v \in V_D,\ \check{v} \in \hat{V} : \gamma_{\Gamma} v = \mathcal{E}_{\Gamma}\check{v} \quad (31)$$

$$\Big\langle \widehat{C}\hat{\psi}, \hat{v} \Big\rangle_{\hat{V}', \hat{V}} = \hat{\alpha}(|\Gamma|\hat{\psi}, \hat{v})_{\Lambda} \qquad \hat{v} \in \hat{V}. \quad (32)$$

The respective adjoints will be denoted as $A^* : V_D \to V_D'$, $\widehat{A}^* : \hat{V} \to \hat{V}'$, $B^* : V_D \to \hat{V}$, $\widehat{B}^* : \hat{V} \to \hat{V}$, $C^* : V_D \to \hat{V}'$, $\widehat{C}^* : \hat{V} \to \hat{V}'$. Let us further define

$$F \in V_D' \text{ s.t. } F(v) = (f, v)_D, \qquad v \in V_D \quad (33)$$

$$G \in \hat{V}' \text{ s.t. } G(\hat{v}) = (|\Sigma|\overline{\overline{g}}, \hat{v})_{\Lambda}, \qquad \hat{v} \in \hat{V}. \quad (34)$$

Equations (24)-(25) can thus be written as:

$$Au - B\overline{\phi} - C\hat{\psi} = F \quad (35)$$

$$\widehat{A}\hat{u} + \widehat{B}\overline{\phi} - \widehat{C}\hat{\psi} = G. \quad (36)$$

If we now consider the space $\mathbb{V} = V_D \times \hat{V}$ and we set $\mathcal{W} = (u, \hat{u}) \in \mathbb{V}$ and $\mathcal{V} = (v, \hat{v}) \in \mathbb{V}$, we can introduce the following operators:

$$\begin{aligned} &\mathcal{A} : \mathbb{V} \to \mathbb{V}' \text{ s.t. } \mathcal{A}(\mathcal{W}, \mathcal{V}) = A(u, v) + \widehat{A}(\tilde{u}, \tilde{v}) \\ &\mathcal{B} : \hat{V}' \to \mathbb{V}' \text{ s.t. } \mathcal{B}(\overline{\phi}, \mathcal{V}) = B(\overline{\phi}, v) - \widehat{B}(\overline{\phi}, \hat{v}) \\ &\mathcal{C} : \hat{V} \to \mathbb{V}' \text{ s.t. } \mathcal{C}(\hat{\psi}, \mathcal{V}) = C(\hat{\psi}, v) + \widehat{C}(\hat{\psi}, \hat{v}) \end{aligned}$$

and the PDE-constrained optimization problem can be written as

$$\min_{(\overline{\phi},\hat{\psi})} J(\overline{\phi},\hat{\psi}) \text{ subject to} \tag{37}$$

$$\mathcal{A}\mathcal{W} - \mathcal{B}\overline{\phi} - \mathcal{C}\hat{\psi} = \mathcal{F}, \tag{38}$$

with $\mathcal{F} \in \mathbb{V}'$ s.t. $\mathcal{F}(\mathcal{V}) = F(v) + G(\hat{v})$.
Let us now provide some results about the optimal control and the stepsize of the steepest descent method for Problem (37)-(38). These results are given in terms of propositions, for the proof of which we refer to the Appendix.

Proposition 1. *Let us consider the trace operator $\gamma_\Gamma : V_D \to \mathcal{H}^\Gamma$ and the extension operators $\mathcal{E}_\Sigma : \hat{V} \to \tilde{V}$ and $\mathcal{E}_\Gamma = \gamma_\Gamma \circ \mathcal{E}_\Sigma : \hat{V} \to \mathcal{H}^\Gamma$, whose respective adjoints are $\gamma_\Gamma^* : \mathcal{H}^{\Gamma\prime} \to V_D'$, ${\mathcal{E}_\Sigma}^* : \tilde{V}' \to \hat{V}'$ and ${\mathcal{E}_\Gamma}^* : \mathcal{H}^{\Gamma\prime} \to \hat{V}'$ and let $\Theta_{\hat{V}} : \hat{V} \to \hat{V}'$ and $\Theta_{\mathcal{H}^\Gamma} : \mathcal{H}^\Gamma \to \mathcal{H}^{\Gamma\prime}$ be Riesz isomorphisms. Then the optimal control $(\overline{\phi},\hat{\psi})$ that provides the solution to (37)-(38) is such that*

$$\Theta_{\hat{V}}(B^*p - \widehat{B}^*\hat{p}) = 0 \tag{39}$$

$$\Theta_{\hat{V}}^{-1}(C^*p + \widehat{C}^*\hat{p} - {\mathcal{E}_\Gamma}^*\Theta_{\mathcal{H}^\Gamma}(\gamma_\Gamma u(\overline{\phi},\hat{\psi}) + \mathcal{E}_\Gamma\hat{u}(\overline{\phi},\hat{\psi}) - 2\mathcal{E}_\Gamma\hat{\psi})) = 0 \tag{40}$$

where $p \in V_D$ and $\hat{p} \in \hat{V}$ are the solutions respectively to

$$A^*p = \gamma_\Gamma^*\Theta_{\mathcal{H}^\Gamma}(\gamma_\Gamma u(\overline{\phi},\hat{\psi}) - \mathcal{E}_\Gamma\hat{\psi}) \tag{41}$$

$$\widehat{A}^*\hat{p} = {\mathcal{E}_\Gamma}^*\Theta_{\mathcal{H}^\Gamma}(\mathcal{E}_\Gamma\hat{u}(\overline{\phi},\hat{\psi}) - \mathcal{E}_\Gamma\hat{\psi}) \tag{42}$$

Starting from the derivatives computed in Proposition 1, let us define the quantities

$$\delta\overline{\phi} = \Theta_{\hat{V}}(B^*p - \widehat{B}^*\hat{p}) \in \hat{V}' \tag{43}$$

$$\delta\hat{\psi} = \Theta_{\hat{V}}^{-1}(C^*p + \widehat{C}^*\hat{p} - {\mathcal{E}_\Gamma}^*\Theta_{\mathcal{H}^\Gamma}(\gamma_\Gamma u(\overline{\phi},\hat{\psi}) + \mathcal{E}_\Gamma\hat{u}(\overline{\phi},\hat{\psi}) - 2\mathcal{E}_\Gamma\hat{\psi})) \in \hat{V}. \tag{44}$$

Then the following proposition holds:

Proposition 2. *Given the variable $\chi = (\overline{\phi},\hat{\psi})$, let us increment it by a step $\zeta\delta\chi$, where $\delta\mathcal{X} = (\delta\overline{\phi},\delta\hat{\psi})$. The steepest descent method corresponds to the stepsize*

$$\zeta = -\frac{\left(\delta\overline{\phi},\delta\overline{\phi}\right)_\Lambda + \left(\delta\hat{\psi},\delta\hat{\psi}\right)_\Lambda}{\left\langle B\delta\overline{\phi} + C\delta\hat{\psi},\delta p\right\rangle_{V_D',V_D} + \left\langle -\widehat{B}\delta\overline{\phi} + \widehat{C}\delta\hat{\psi},\delta\hat{p}\right\rangle_{\hat{V}',\hat{V}} - \left\langle {\mathcal{E}_\Gamma}^*\Theta_{\mathcal{H}^\Gamma}(\gamma_\Gamma\delta u + \mathcal{E}_\Gamma\delta\hat{u} - 2\mathcal{E}_\Gamma\delta\hat{\psi}),\delta\hat{\psi}\right\rangle_{\hat{V}',\hat{V}}}$$

where

$$\delta u = u(\delta\overline{\phi},\delta\hat{\psi}) = A^{-1}(B\delta\overline{\phi} + C\delta\hat{\psi}) \in V_D,$$
$$\delta\hat{u} = \hat{u}(\delta\overline{\phi},\delta\hat{\psi}) = \widehat{A}^{-1}(-\widehat{B}\delta\overline{\phi} + \widehat{C}\delta\hat{\psi}) \in \hat{V}$$

and $\delta p \in V_D$, $\delta\hat{p} \in \hat{V}$ are such that:

$$A^*\delta p = \gamma_\Gamma^* \Theta_{\mathcal{H}^\Gamma}(\gamma_\Gamma \delta u - \mathcal{E}_\Gamma \delta\hat{\psi})$$
$$\widehat{A}^*\delta\hat{p} = \mathcal{E}_\Gamma{}^* \Theta_{\mathcal{H}^\Gamma}(\mathcal{E}_\Gamma \delta\hat{u} - \mathcal{E}_\Gamma \delta\hat{\psi})$$

5. Managing multiple cylinders and their intersections

The previous discussion can be readily adapted to the case of multiple, say $\mathcal{I}$, small cylindrical inclusions Σ_i, with lateral surface Γ_i and centreline Λ_i, $i = 1, \ldots, \mathcal{I}$. Let us first assume that the inclusions are disjoint, i.e. $\Sigma_k \cap \Sigma_j = \emptyset$ for $k \neq j = 1, \ldots \mathcal{I}$. Function spaces $\hat{V}$, $\widetilde{V}$, $\mathcal{H}^\Gamma$ are introduced on each segment and denoted by $\hat{V}_i$, $\widetilde{V}_i$, $\mathcal{H}^{\Gamma_i}$, while trace operator γ_Γ, extension operator $\mathcal{E}_\Gamma$ and $\mathcal{E}_\Sigma$ are easily re-defined for each segment and denoted by γ_{Γ_i}, $\mathcal{E}_{\Gamma_i}$ and $\mathcal{E}_{\Sigma_i}$, respectively. Operators (27)-(32) are re-written as:

$$\langle Au, v\rangle_{V_D', V_D} = (K\nabla u, \nabla v)_D + \alpha \sum_{i=1}^{\mathcal{I}} (|\Gamma_i| \check{u}_i, \check{v}_i)_{\Lambda_i}$$
$$\forall v \in V_D,\ \check{v}_i \in \hat{V}_i : \gamma_{\Gamma_i} v = \mathcal{E}_{\Gamma_i} \check{v}_i, \forall i = 1, \ldots, \mathcal{I}$$
$$\left\langle \widehat{A}_i \hat{u}_i, \hat{v}_i \right\rangle_{\hat{V}_i', \hat{V}_i} = \left(\tilde{K}_i |\Sigma_i| \frac{d\hat{u}_i}{ds}, \frac{d\hat{v}_i}{ds} \right)_{\Lambda_i} + \hat{\alpha}(|\Gamma_i| \hat{u}_i, \hat{v}_i)_{\Lambda_i} \qquad \forall \hat{v}_i \in \hat{V}_i$$

$$\left\langle B_i \overline{\phi_i}, v_i \right\rangle_{V_D', V_D} = \left\langle |\Gamma_i| \overline{\phi}_i, \check{v}_i \right\rangle_{\hat{V}_i', \hat{V}_i} \qquad \forall v \in V : \gamma_{\Gamma_i} v = \mathcal{E}_{\Gamma_i} \check{v}_i,\ \check{v}_i \in \hat{V}_i$$
$$\left\langle \widehat{B}_i \overline{\phi}_i, \hat{v} \right\rangle_{\hat{V}_i', \hat{V}_i} = \left\langle |\Gamma_i| \overline{\phi}_i, \hat{v} \right\rangle_{\hat{V}_i', \hat{V}_i} \qquad \forall \hat{v} \in \hat{V}_i$$

$$\left\langle C_i \hat{\psi}_i, v \right\rangle_{V_D', V_D} = \alpha(|\Gamma_i| \hat{\psi}, \check{v})_{\Lambda_i} \qquad \forall v \in V_D,\ \check{v}_i \in \hat{V}_i : \gamma_{\Gamma_i} v = \mathcal{E}_{\Gamma_i} \check{v}$$
$$\left\langle \widehat{C}_i \hat{\psi}_i, \hat{v} \right\rangle_{\hat{V}_i', \hat{V}_i} = \hat{\alpha}(|\Gamma_i| \hat{\psi}_i, \hat{v})_{\Lambda_i} \qquad \hat{v} \in \hat{V}_i.$$

Problem (35)-(36) can be finally re-written for an arbitrary set of $\mathcal{I}$ centrelines as:

$$Au - B_i \overline{\phi}_i - C_i \hat{\psi}_i = F \tag{45}$$
$$\widehat{A}_i \hat{u}_i + \widehat{B}_i \overline{\phi}_i - \widehat{C}_i \hat{\psi}_i = G_i, \tag{46}$$

in which we consider different 1D variables $\hat{u}_i$, $\overline{\phi}_i$, $\hat{\psi}_i$ on the different 1D domains. The definition of G_i follows from the definition of an operator in the form of (34) for each segment.

In case cylindrical inclusions with centrelines intersecting in a point, i.e. such that $\bar{\Lambda}_i \cap \bar{\Lambda}_j = P_\zeta$, $i, j \in [1, \ldots, \mathcal{I}]$, we can still adopt formulation (45)-(46) by splitting the intersecting centrelines into non intersecting sub-segments and

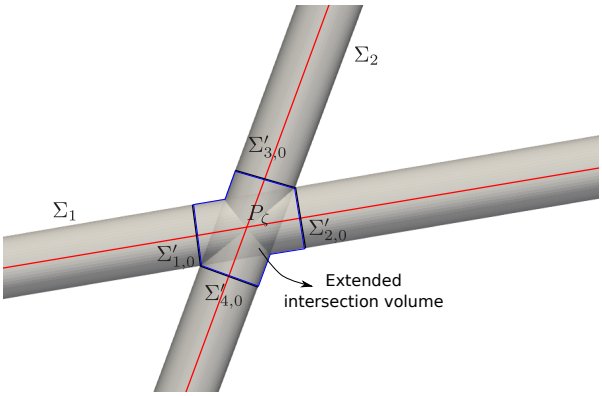

Figure 1: Two intersecting cylinders Σ_1 and Σ_2

then adding continuity conditions at the intersection points P_ζ. The considered situation is depicted in Figure 1, in which an *extended intersection volume* is highlighted. According to model assumptions, in this volume the solution has a unique constant value, coinciding with the value in P_ζ, and the extension and trace operators γ_{Γ_i}, $\mathcal{E}_{\Gamma_i}$ and $\mathcal{E}_{\Sigma_i}$ are still well defined for the two original cylinders. Faces $\Sigma'_{k,0}$, $k = 1, \dots, 4$, belonging to the boundary of the extended intersection volume, can be considered as the extreme sections of the four sub-cylinders. We need however to assume that the diameter of the extended intersection volume, defined as the maximum distance between two points belonging to the volume, is small if compared to the minimum length of the intersecting inclusions. Different intersection modes, such as, e.g. cylinders with intersecting lateral surfaces and non-intersecting centrelines, or cylinders with (partially) overlapping centrelines, are, instead, excluded.

Finally, the cost functional is re-written as:

$$J = \sum_{i=1}^{\mathcal{I}} J_i := \sum_{k=1}^{\mathcal{I}} \frac{1}{2} \left(||\gamma_{\Gamma_i} u(\overline{\phi}_i, \hat{\psi}_i) - \psi_i||^2_{\mathcal{H}^\Gamma} + ||\gamma_\Gamma \tilde{u}_i(\overline{\phi}_i, \hat{\psi}_i) - \psi_i||^2_{\mathcal{H}^\Gamma} \right) \quad (47)$$

where $\tilde{u}_i = \mathcal{E}_{\Sigma_i} \hat{u}_i$ and $\psi_i = \mathcal{E}_{\Gamma_i} \hat{\psi}_i$.

6. Discrete matrix formulation

Here the discrete matrix form of problem (37)-(38) is presented. The 3D-1D coupling is trivial in the discrete approximation spaces, given the regularity properties of the function spaces commonly used for discretization. Nonetheless, the present approach has the advantage of having a well posed mathematical formulation, and it even allows the use of non conforming meshes at the interfaces of the subdomains. Indeed, thanks to the optimization framework, it is possible to use completely independent meshes for the various domains and also for the interface variables, without any theoretical constraint on mesh sizes.

For the sake of generality we will consider, from the beginning, the presence of multiple segments crossing domain Ω. Let us consider $\mathcal{I}$ segments of different length and orientation, defined ad $\Lambda_i = \{\boldsymbol{\lambda}_i(s), s \in (0, S_i)\}$, $i = 1, ..., \mathcal{I}$. Let us extend the domain D to the whole Ω and let us consider a tetrahedral mesh $\mathcal{T}$ of domain Ω, and let us define, on this mesh, Lagrangian finite element basis functions $\{\varphi_k\}_{k=1}^N$, such that $U = \sum_{k=1}^N U_k \varphi_k$ is the discrete approximation of pressure u. Let us then build three partitions of each segment Λ_i, named $\hat{\mathcal{T}}_i$, τ_i^ϕ and τ_i^ψ, defined independently from each other and from $\mathcal{T}$. Let us further define the basis functions $\{\hat{\varphi}_{i,k}\}_{k=1}^{\hat{N}_i}$ on $\hat{\mathcal{T}}_i$, $\{\theta_{i,k}\}_{k=1}^{N_i^\phi}$ on τ_i^ϕ and $\{\eta_{i,k}\}_{k=1}^{N_i^\psi}$ on τ_i^ψ, with $\hat{N}_i$, N_i^ϕ and N_i^ψ denoting the number of DOFs of the discrete approximations of the variables $\hat{u}_i$, $\overline{\phi}_i$ and $\hat{\psi}_i$ respectively, having set:

$$\hat{U}_i = \sum_{k=1}^{\hat{N}_i} \hat{U}_{i,k} \hat{\varphi}_{i,k}, \quad \Phi_i = \sum_{k=1}^{N_i^\phi} \Phi_{i,k} \theta_{i,k}, \quad \Psi_i = \sum_{k=1}^{N_i^\psi} \Psi_{i,k} \eta_{i,k}$$

We then define the following matrices:

$$\boldsymbol{A} \in \mathbb{R}^{N \times N} \text{ s.t. } (A)_{kl} = \int_\Omega \boldsymbol{K} \nabla \varphi_k \nabla \varphi_l \, d\omega + \alpha \sum_{i=1}^{\mathcal{I}} \int_{\Lambda_i} |\Gamma(s_i)| \varphi_{k|_{\Lambda_i}} \varphi_{l|_{\Lambda_i}} ds$$

$$\hat{\boldsymbol{A}}_{\boldsymbol{i}} \in \mathbb{R}^{\hat{N}_i \times \hat{N}_i} \text{ s.t. } (\hat{A}_i)_{kl} = \int_{\Lambda_i} \tilde{\boldsymbol{K}}_{\boldsymbol{i}} |\Sigma(s_i)| \frac{d\hat{\varphi}_{i,k}}{ds} \frac{d\hat{\varphi}_{i,l}}{ds} \, ds + \hat{\alpha} \int_{\Lambda_i} |\Gamma(s_i)| \hat{\varphi}_{i,k} \hat{\varphi}_{i,l} \, ds$$

$$\boldsymbol{B}_{\boldsymbol{i}} \in \mathbb{R}^{N \times N_i^\phi} \text{ s.t. } (B_i)_{kl} = \int_{\Lambda_i} |\Gamma(s_i)| \varphi_{k|_{\Lambda_i}} \theta_{i,l} \, ds$$

$$\hat{\boldsymbol{B}}_{\boldsymbol{i}} \in \mathbb{R}^{\hat{N}_i \times N_i^\phi} \text{ s.t. } (\hat{B}_i)_{kl} = \int_{\Lambda_i} |\Gamma(s_i)| \hat{\varphi}_{i,k} \, \theta_{i,l} \, ds$$

$$\boldsymbol{C}_{\boldsymbol{i}}^\alpha \in \mathbb{R}^{N \times N_i^\psi} \text{ s.t. } (C_i^\alpha)_{kl} = \alpha \int_{\Lambda_i} |\Gamma(s_i)| \varphi_{k|_{\Lambda_i}} \eta_{i,l} \, ds$$

$$\hat{\boldsymbol{C}}_{\boldsymbol{i}}^\alpha \in \mathbb{R}^{\hat{N}_i \times N_i^\psi} \text{ s.t. } (\hat{C}_i^{\,\alpha})_{kl} = \hat{\alpha} \int_{\Lambda_i} |\Gamma(s_i)| \hat{\varphi}_{i,k} \, \eta_{i,l} \, ds,$$

and the vectors

$$f \in \mathbb{R}^N \text{ s.t. } f_k = \int_\Omega f \varphi_k \, d\omega$$

$$g_i \in \mathbb{R}^{\hat{N}_i} \text{ s.t. } (g_i)_k = \int_{\Lambda_i} |\Sigma(s_i)| \overline{\overline{g}} \, \hat{\varphi}_{i,k} \, ds.$$

Setting $\hat{N} = \sum_{i=1}^{\mathcal{I}} \hat{N}_i$, $N^\psi = \sum_{i=1}^{\mathcal{I}} N_i^\psi$ and $N^\phi = \sum_{i=1}^{\mathcal{I}} N_i^\phi$, we can group the matrices as follows for all the segments in the domain:

$$\boldsymbol{B} = [\boldsymbol{B_1}, \boldsymbol{B_2}, ..., \boldsymbol{B_{\mathcal{I}}}] \in \mathbb{R}^{N \times N^\phi} \qquad \hat{\boldsymbol{B}} = \text{diag}\left(\hat{\boldsymbol{B}}_{\boldsymbol{1}}, ..., \hat{\boldsymbol{B}}_{\boldsymbol{\mathcal{I}}}\right) \in \mathbb{R}^{\hat{N} \times N^\phi}$$

$$\boldsymbol{C}^\alpha = [\boldsymbol{C}_{\boldsymbol{1}}^\alpha, \boldsymbol{C}_{\boldsymbol{2}}^\alpha, ..., \boldsymbol{C}_{\boldsymbol{\mathcal{I}}}^\alpha] \in \mathbb{R}^{N \times N^\psi} \qquad \hat{\boldsymbol{C}}^\alpha = diag\left(\hat{\boldsymbol{C}}_{\boldsymbol{1}}^\alpha, ..., \hat{\boldsymbol{C}}_{\boldsymbol{\mathcal{I}}}^\alpha\right) \in \mathbb{R}^{\hat{N} \times N^\psi}$$

and, for non intersecting segments, we have:

$$\hat{\boldsymbol{A}} = \text{diag}\left(\hat{\boldsymbol{A}}_{\boldsymbol{1}}, ..., \hat{\boldsymbol{A}}_{\boldsymbol{\mathcal{I}}}\right) \in \mathbb{R}^{\hat{N}\times\hat{N}},$$

whereas, for groups of intersecting segments, we proceed as described in Section 5 and we enforce continuity through Lagrange multipliers. For each connected group of segments we thus have:

$$\hat{\boldsymbol{A}}^{\star}_{\boldsymbol{\zeta}} = \begin{bmatrix} \text{diag}\left(\hat{\boldsymbol{A}}_{\boldsymbol{\zeta_1}}, ..., \hat{\boldsymbol{A}}_{\boldsymbol{\zeta_n}}\right) & \boldsymbol{Q}^T \\ \boldsymbol{Q} & \boldsymbol{0} \end{bmatrix}$$

where matrix $\boldsymbol{Q}$ simply equates the DOFs at the extrema of connected subsegments. Matrices $\hat{\boldsymbol{A}}^{\star}_{\boldsymbol{\zeta}}$, for ζ spanning the whole number of connected groups of segments, are assembled block diagonally to form matrix $\hat{\boldsymbol{A}}$. Please note that, for disconnected segments, each matrix $\hat{\boldsymbol{A}}^{\star}_{\boldsymbol{\zeta}}$ coincides with matrix $\hat{\boldsymbol{A}}_{\boldsymbol{\zeta}}$. Finally we can write

$$\boldsymbol{A}U - \boldsymbol{B}\Phi - \boldsymbol{C}^{\alpha}\Psi = f \tag{48}$$

$$\hat{\boldsymbol{A}}\hat{U} + \hat{\boldsymbol{B}}\Phi - \hat{\boldsymbol{C}}^{\alpha}\Psi = g \tag{49}$$

with

$$\hat{U} = \left[\hat{U}_1^T, ..., \hat{U}_{\mathcal{I}}^T\right]^T \in \mathbb{R}^{\hat{N}}; \quad g = [g_1^T, g_2^T, ..., g_{\mathcal{I}}^T]^T \in \mathbb{R}^{\hat{N}}$$

$$\Phi = \left[\Phi_1^T, ..., \Phi_{\mathcal{I}}^T\right]^T \in \mathbb{R}^{N^{\phi}}; \quad \Psi = \left[\Psi_1^T, ..., \Psi_{\mathcal{I}}^T\right]^T \in \mathbb{R}^{N^{\psi}}.$$

In order to get a more compact form of the previous equations, let us set $W = (U, \hat{U})$ and

$$\boldsymbol{\mathcal{A}} = \begin{bmatrix} \boldsymbol{A} & 0 \\ 0 & \hat{\boldsymbol{A}} \end{bmatrix}, \qquad \boldsymbol{\mathcal{B}} = \begin{bmatrix} \boldsymbol{B} \\ -\hat{\boldsymbol{B}} \end{bmatrix}, \qquad \boldsymbol{\mathcal{C}}^{\alpha} = \begin{bmatrix} \boldsymbol{C}^{\alpha} \\ \hat{\boldsymbol{C}}^{\alpha} \end{bmatrix} \qquad \mathcal{F} = \begin{bmatrix} f \\ g \end{bmatrix}, \tag{50}$$

so that the discrete constraint equations become:

$$\boldsymbol{\mathcal{A}}W - \boldsymbol{\mathcal{B}}\Phi - \boldsymbol{\mathcal{C}}^{\alpha}\Psi = \mathcal{F}. \tag{51}$$

Concerning the cost functional in (26), first we define matrices

$$\boldsymbol{G_i} \in \mathbb{R}^{N\times N} \text{ s.t. } (G_i)_{kl} = \int_{\Lambda_i} \varphi_{k|_{\Lambda_i}} \varphi_{l|_{\Lambda_i}} ds$$

$$\hat{\boldsymbol{G}}_{\boldsymbol{i}} \in \mathbb{R}^{\hat{N}_i\times\hat{N}_i} \text{ s.t. } (\hat{G}_i)_{kl} = \int_{\Lambda_i} \hat{\varphi}_{i,k}\ \hat{\varphi}_{i,l}\ ds$$

$$\boldsymbol{G}^{\boldsymbol{\psi}}_{\boldsymbol{i}} \in \mathbb{R}^{N_i^{\psi}\times N_i^{\psi}} \text{ s.t. } (G_i^{\psi})_{kl} = \int_{\Lambda_i} \eta_{i,k}\ \eta_{i,l}\ ds$$

$$\boldsymbol{C_i} \in \mathbb{R}^{N\times N_i^{\psi}} \text{ s.t. } (C_i)_{kl} = \int_{\Lambda_i} \varphi_{k|_{\Lambda_i}} \eta_{i,l}\ ds$$

$$\hat{\boldsymbol{C}}_{\boldsymbol{i}} \in \mathbb{R}^{\hat{N}_i\times N_i^{\psi}} \text{ s.t. } (\hat{C}_i)_{kl} = \int_{\Lambda_i} \hat{\varphi}_{i,k}\ \eta_{i,l}\ ds$$

and then

$$\boldsymbol{G} = \sum_{i=1}^{\mathcal{I}} \boldsymbol{G}_i \in \mathbb{R}^{N\times N} \qquad \hat{\boldsymbol{G}} = \text{diag}\left(\hat{\boldsymbol{G}}_{\boldsymbol{1}}^T, ..., \hat{\boldsymbol{G}}_{\boldsymbol{\mathcal{I}}}^T\right) \in \mathbb{R}^{\hat{N}\times\hat{N}} \qquad \boldsymbol{\mathcal{G}} = \begin{bmatrix} \boldsymbol{G} & 0 \\ 0 & \hat{\boldsymbol{G}} \end{bmatrix}$$
$$\boldsymbol{G}^{\boldsymbol{\psi}} = \text{diag}\left(\boldsymbol{G}_{\boldsymbol{1}}^{\boldsymbol{\psi}}, ..., \boldsymbol{G}_{\boldsymbol{\mathcal{I}}}^{\boldsymbol{\psi}}\right) \in \mathbb{R}^{N^\psi\times N^\psi} \tag{52}$$

$$\boldsymbol{C} = [\boldsymbol{C_1}, \boldsymbol{C_2}, ..., \boldsymbol{C_{\mathcal{I}}}] \in \mathbb{R}^{N\times N^\psi} \quad \hat{\boldsymbol{C}} = \text{diag}\left(\hat{\boldsymbol{C}}_{\boldsymbol{1}}, ..., \hat{\boldsymbol{C}}_{\boldsymbol{\mathcal{I}}}\right) \in \mathbb{R}^{\hat{N}\times N^\psi} \quad \boldsymbol{\mathcal{C}} = \begin{bmatrix} \boldsymbol{C} \\ \hat{\boldsymbol{C}} \end{bmatrix}.$$

The discrete cost functional then reads:

$$\tilde{J} = \frac{1}{2}\left(U^T\boldsymbol{G}U - U^T\boldsymbol{C}\Psi - \Psi^T\boldsymbol{C}^TU + \hat{U}^T\hat{\boldsymbol{G}}\hat{U} - \hat{U}^T\hat{\boldsymbol{C}}\Psi - \Psi^T\hat{\boldsymbol{C}}^T\hat{U} + 2\Psi^T\boldsymbol{G}^{\boldsymbol{\psi}}\Psi\right) =$$
$$= \frac{1}{2}\left(W^T\boldsymbol{\mathcal{G}}W - W^T\boldsymbol{\mathcal{C}}\Psi - \Psi^T\boldsymbol{\mathcal{C}}^TW + 2\Psi^T\boldsymbol{G}^{\boldsymbol{\psi}}\Psi\right). \tag{53}$$

The discrete matrix formulation of the 3D-1D problem finally takes the form:

$$\min_{(\Phi,\Psi)} \tilde{J}(\Phi,\Psi) \text{ subject to (51)}. \tag{54}$$

First order optimality conditions for the above problem correspond to the saddle-point system:

$$\boldsymbol{\mathcal{S}} = \begin{bmatrix} \boldsymbol{\mathcal{G}} & \boldsymbol{0} & -\boldsymbol{\mathcal{C}} & \boldsymbol{\mathcal{A}}^T \\ \boldsymbol{0} & \boldsymbol{0} & \boldsymbol{0} & \boldsymbol{\mathcal{B}}^T \\ -\boldsymbol{\mathcal{C}}^T & \boldsymbol{0} & 2\boldsymbol{G}^{\boldsymbol{\psi}} & (-\boldsymbol{\mathcal{C}}^{\boldsymbol{\alpha}})^T \\ \boldsymbol{\mathcal{A}} & \boldsymbol{\mathcal{B}} & -\boldsymbol{\mathcal{C}}^{\boldsymbol{\alpha}} & \boldsymbol{0} \end{bmatrix} \tag{55}$$

$$\boldsymbol{\mathcal{S}} \begin{bmatrix} W \\ \Phi \\ \Psi \\ -P \end{bmatrix} = \begin{bmatrix} \mathcal{F} \\ \boldsymbol{0} \\ \boldsymbol{0} \\ \boldsymbol{0} \end{bmatrix} \tag{56}$$

Proposition 3. *Matrix $\boldsymbol{\mathcal{S}}$ in* (55) *is non-singular and the unique solution of* (56) *is equivalent to the solution of the optimization problem* (54)*.*

The proof of Proposition 3 derives from classical arguments of quadratic programming once the following lemma is proven:

Lemma 1. *Let matrix $\boldsymbol{\mathcal{A}}^\star \in \mathbb{R}^{(N+\hat{N})\times(N+\hat{N}+N^\phi+N^\psi)}$ be as*

$$\boldsymbol{\mathcal{A}}^\star = \begin{bmatrix} \boldsymbol{\mathcal{A}} & \boldsymbol{\mathcal{B}} & -\boldsymbol{\mathcal{C}}^{\boldsymbol{\alpha}} \end{bmatrix}$$

and let $\boldsymbol{\mathcal{G}}^\star \in \mathbb{R}^{(N+\hat{N}+N^\phi+N^\psi)\times(N+\hat{N}+N^\phi+N^\psi)}$ be defined as

$$\boldsymbol{\mathcal{G}}^\star = \begin{bmatrix} \boldsymbol{\mathcal{G}} & \boldsymbol{0} & -\boldsymbol{\mathcal{C}} \\ \boldsymbol{0} & \boldsymbol{0} & \boldsymbol{0} \\ -\boldsymbol{\mathcal{C}}^T & \boldsymbol{0} & 2\boldsymbol{G}^{\boldsymbol{\psi}} \end{bmatrix}$$

Then matrix $\boldsymbol{\mathcal{A}}^\star$ is full rank and matrix $\boldsymbol{\mathcal{G}}^\star$ is symmetric positive definite on $\ker(\boldsymbol{\mathcal{A}}^\star)$*.*

Proof. The proof is adapted from the one provided in [21], we report here the key steps. Matrix $\boldsymbol{\mathcal{A}}$ is full rank and matrix $\boldsymbol{\mathcal{G}}^\star$ is symmetric positive semi-definite by construction. We thus need to show that $\ker(\boldsymbol{\mathcal{G}}^\star) \cap \ker(\boldsymbol{\mathcal{A}}^\star) = \{0\}$. Let us consider the canonical basis for $\mathbb{R}^{N^\Phi + N^\Psi}$ and let e_k denote the k-th element of such basis, $k = 1, \ldots, N^\Phi + N^\Psi$. Let $z_k \in \ker(\boldsymbol{\mathcal{A}}^\star)$ be defined as:

$$z_k = \begin{bmatrix} \boldsymbol{\mathcal{A}}^{-1} \begin{bmatrix} \boldsymbol{\mathcal{B}} & -\boldsymbol{\mathcal{C}}^\alpha \end{bmatrix} e_k \\ e_k \end{bmatrix}.$$

Let us assume that $1 \leq k \leq N^\Phi$, thus corresponding to a non null value of the variable Φ on one segment. This in turn gives a non null value U and $\hat{U}$ on the traces and thus a non null value of the functional, or $z_k^T \boldsymbol{\mathcal{G}}^\star z_k > 0$. If instead $N^\Phi + 1 \leq k \leq N^\Psi$, this corresponds to a non-null variable $\Psi := e_k$. Since the solution to (56) is the same for every value of α and $\hat{\alpha}$, included $\alpha = \hat{\alpha} = 0$ (the consistent terms depending on α and $\hat{\alpha}$ are only required for the independent resolution on the sub-domains [24]), we choose here $\alpha = \hat{\alpha} = 0$, so that:

$$z_k = \begin{bmatrix} \boldsymbol{\mathcal{A}}^{-1} \begin{bmatrix} \boldsymbol{\mathcal{B}} & \mathbf{0} \end{bmatrix} e_k \\ e_k \end{bmatrix} := \begin{bmatrix} \mathbf{0} \\ e_k \end{bmatrix}$$

thus U, $\hat{U}$ are null, and therefore we can conclude that $z_k^T \boldsymbol{\mathcal{G}} z_k > 0$ also in this case (see [21] for the proof with $\alpha, \hat{\alpha} > 0$). Summarizing we have shown that $z_k \notin \ker(\boldsymbol{\mathcal{G}}^\star)$ for any $k = 1, \ldots, N^\Phi + N^\Psi$. The vector space $\ker(\boldsymbol{\mathcal{A}}^\star) = \text{span}\{z_1, \ldots, z^{N^\Phi + N^\Psi}\}$ is a subspace of $\text{Im}(\boldsymbol{\mathcal{G}}^\star)$, and $\ker(\boldsymbol{\mathcal{G}}^\star) \cap \ker(\boldsymbol{\mathcal{A}}^\star) = \{\mathbf{0}\}$. □

System (56) can be used to obtain a numerical solution to problem (54). For very large problems instead, the above system might become computationally expensive to solve, and thus an alternative resolution strategy is proposed, as described below, which allows the use of iterative solvers and is ready for parallel implementation. By formally replacing $W = \boldsymbol{\mathcal{A}}^{-1}(\boldsymbol{\mathcal{B}}\Phi - \boldsymbol{\mathcal{C}}^\alpha \Psi + \mathcal{F})$ in the

functional (53), we obtain

$$
\begin{aligned}
J^\star(\Phi,\Psi) = \frac{1}{2}\Big(& (\boldsymbol{\mathcal{A}}^{-1}\boldsymbol{\mathcal{B}}\Phi + \boldsymbol{\mathcal{A}}^{-1}\boldsymbol{\mathcal{C}}^\alpha\Psi + \boldsymbol{\mathcal{A}}^{-1}\mathcal{F})^T\boldsymbol{\mathcal{G}}(\boldsymbol{\mathcal{A}}^{-1}\boldsymbol{\mathcal{B}}\Phi + \boldsymbol{\mathcal{A}}^{-1}\boldsymbol{\mathcal{C}}^\alpha\Psi + \boldsymbol{\mathcal{A}}^{-1}\mathcal{F}) + \\
& - (\boldsymbol{\mathcal{A}}^{-1}\boldsymbol{\mathcal{B}}\Phi + \boldsymbol{\mathcal{A}}^{-1}\boldsymbol{\mathcal{C}}^\alpha\Psi + \boldsymbol{\mathcal{A}}^{-1}\mathcal{F})^T\boldsymbol{\mathcal{C}}\Psi + \\
& - \Psi^T\boldsymbol{\mathcal{C}}^T(\boldsymbol{\mathcal{A}}^{-1}\boldsymbol{\mathcal{B}}\Phi + \boldsymbol{\mathcal{A}}^{-1}\boldsymbol{\mathcal{C}}^\alpha\Psi + \boldsymbol{\mathcal{A}}^{-1}\mathcal{F})\Big) = \\
= \frac{1}{2}\begin{bmatrix}\Phi^T & \Psi^T\end{bmatrix} & \begin{bmatrix} \boldsymbol{\mathcal{B}}^T\boldsymbol{\mathcal{A}}^{-T}\boldsymbol{\mathcal{G}}\boldsymbol{\mathcal{A}}^{-1}\boldsymbol{\mathcal{B}} & \boldsymbol{\mathcal{B}}^T\boldsymbol{\mathcal{A}}^{-T}\boldsymbol{\mathcal{G}}\boldsymbol{\mathcal{A}}^{-1}\boldsymbol{\mathcal{C}}^\alpha + \\ & -\boldsymbol{\mathcal{B}}^T\boldsymbol{\mathcal{A}}^{-T}\boldsymbol{\mathcal{C}} \\ (\boldsymbol{\mathcal{C}}^\alpha)^T\boldsymbol{\mathcal{A}}^{-T}\boldsymbol{\mathcal{G}}\boldsymbol{\mathcal{A}}^{-1}\boldsymbol{\mathcal{B}} + & (\boldsymbol{\mathcal{C}}^\alpha)^T\boldsymbol{\mathcal{A}}^{-T}\boldsymbol{\mathcal{G}}\boldsymbol{\mathcal{A}}^{-1}\boldsymbol{\mathcal{C}}^\alpha + \\ -\boldsymbol{\mathcal{C}}^T\boldsymbol{\mathcal{A}}^{-1}\boldsymbol{\mathcal{B}} & -\boldsymbol{\mathcal{C}}^T\boldsymbol{\mathcal{A}}^{-T}\boldsymbol{\mathcal{C}}^\alpha + \\ & -(\boldsymbol{\mathcal{C}}^\alpha)^T\boldsymbol{\mathcal{A}}^{-1}\boldsymbol{\mathcal{C}} + 2\boldsymbol{\mathcal{G}}^\psi \end{bmatrix}\begin{bmatrix}\Phi \\ \\ \Psi\end{bmatrix} + \\
& + \mathcal{F}^T\begin{bmatrix}\boldsymbol{\mathcal{A}}^{-T}\boldsymbol{\mathcal{G}}\boldsymbol{\mathcal{A}}^{-1}\boldsymbol{\mathcal{B}} & \boldsymbol{\mathcal{A}}^{-T}\boldsymbol{\mathcal{G}}\boldsymbol{\mathcal{A}}^{-1}\boldsymbol{\mathcal{C}}^\alpha - \boldsymbol{\mathcal{A}}^{-T}\boldsymbol{\mathcal{C}}\end{bmatrix}\begin{bmatrix}\Phi \\ \Psi\end{bmatrix} + \\
& + \frac{1}{2}\Big(\mathcal{F}^T\boldsymbol{\mathcal{A}}^{-T}\boldsymbol{\mathcal{G}}\boldsymbol{\mathcal{A}}^{-1}\mathcal{F}\Big) = \\
= \frac{1}{2}\big(\mathcal{X}^T\boldsymbol{M}\mathcal{X} + 2d^T\mathcal{X} + q\big)\,. & \qquad (57)
\end{aligned}
$$

Matrix $\boldsymbol{M}$ is symmetric positive definite as follows from the equivalence of this formulation with the previous saddle point system (56), and thus the minimization of the unconstrained problem (57) can be performed via a gradient based scheme. It is however to remark that the computation of gradient direction at point $\mathcal{X}^\sharp$, i.e. $\nabla J^\star(\mathcal{X}^\sharp) = \boldsymbol{M}\mathcal{X}^\sharp + d$, can be performed in a matrix free format and involves the independent factorization of the 1D matrices $\hat{\boldsymbol{A}}_{\boldsymbol{i}}$, $i = 1,\dots,L$ and of the 3D elliptic matrix $\boldsymbol{A}$, which are all non singular as long as $\alpha, \hat{\alpha} > 0$, thus allowing for parallel computing. It is to remark that saddle point matrices as the one in (55) can be ill conditioned. The use of a resolution strategy based on a gradient based scheme for the minimization of the unconstrained functional is expected to result in a problem with a mitigated condition number, actually coinciding with the application of a null-space based preconditioning technique [29]. The analysis of this solving strategy and of its potential for parallel computing is deferred to a forthcoming work.

7. Numerical results

In this section we propose some numerical test to validate the proposed approach and to show its applicability to the problem of interest. Three numerical tests are proposed. A first problem called *Test Problem 1* (TP1) takes into account a single cylindrical inclusion and has a smooth analytical solution, thus allowing to evaluate convergence trends for the error. The second test, called *Test Problem 2* (TP2), takes into account a different problem with no known analytical solution on a similar geometry. In this case, the obtained solution is compared to a 3D-3D simulation with standard conforming finite elements, and

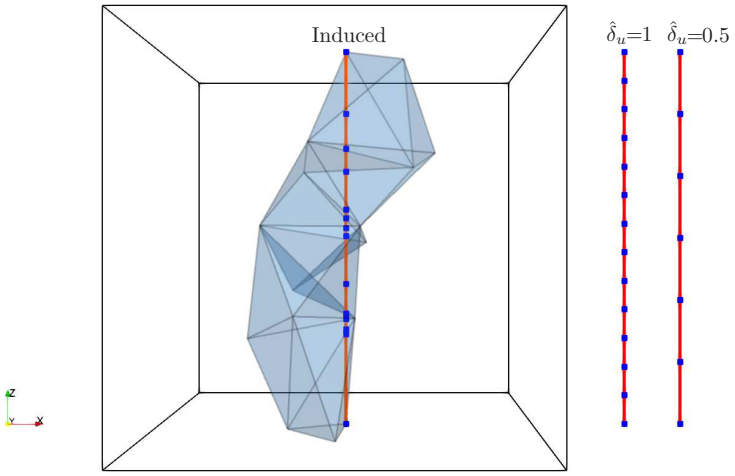

Figure 2: Highlight on the tetrahedra intersected by a segment and consequently induced mesh; on the right equispaced partitions of the segment for $\hat{\delta}_u = 1$ and for $\hat{\delta}_u = 0.5$.

different values of the coefficient $\tilde{K}$ are considered. Finally an example with multiple intersecting inclusions is proposed, to test the behavior of the method in more general settings. In this case, a qualitative evaluation on the behavior of the numerical solution is proposed, along with a quantitative evaluation of a proposed error indicator.

All the simulations are performed using finite elements on 3D and 1D non-conforming meshes, independently generated on the sub-domains. A mesh parameter h is used to denote the maximum diameter of the tetrahedra for the 3D mesh of Ω, whereas the refinement level of the 1D meshes $\hat{\mathcal{T}}_i$, τ_i^{ϕ}, τ_i^{ψ}, $i = 1, ...\mathcal{I}$, is provided in relation to the mesh-size of the 1D mesh induced on the segments Λ_i by the tetrahedral mesh, i.e. the 1D mesh given by the intersections of Λ_i with the tetrahedra in $\mathcal{T}$, see Figure 2. This is done in order to better highlight the relative sizes of the various meshes. In particular the non-dimensional number $\hat{\delta}_{u,i}$ denotes the ratio between the number of elements of the mesh in $\hat{\mathcal{T}}_i$ with respect to the number of elements of the induced mesh on Λ_i, whereas $\delta_{\phi,i}$ and $\delta_{\psi,i}$ the ratio between the number of elements in τ_i^{ϕ}, τ_i^{ψ}, respectively, and the induced mesh. Figure 2 shows the induced mesh, in the middle, and two 1D meshes, e.g. for $\hat{\mathcal{T}}$ corresponding to values of $\hat{\delta}_u = 1$ and $\hat{\delta}_u = 0.5$ and equally-spaced nodes. In the simulations, for simplicity, we will always use equally-spaced nodes for the 1D meshes and unique different values of $\hat{\delta}_u$, δ_{ϕ} and δ_{ψ} for the various segments, thus dropping, in the following, the reference to segment index for these parameters. Even when it is not used for the description of any 1D variable, the induced mesh is used for the computation of the integrals between the basis functions of the 1D variables and the trace on each segment of the 3D basis functions. Linear Lagrangian finite elements are used on $\mathcal{T}$, $\hat{\mathcal{T}}_i$, τ_i^{ψ}, whereas piece-wise constant basis functions are used to describe variables

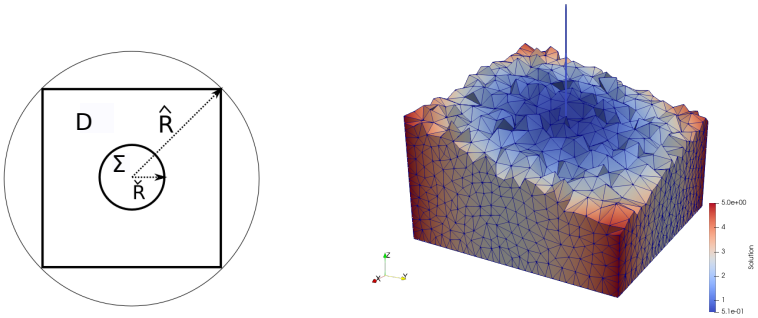

Figure 3: TP1: on the left, section view of the starting 3D-3D domain for the TestProblem1 experiment; on the right solution obtained inside the cube and on the segment for $h = 0.086$, $\hat{\delta}_u = 1$, $\delta_\phi = 0.5$ and $\delta_\psi = 0.5$.

ϕ_i on τ_i^ϕ, $i = 1, ...\mathcal{I}$. All numerical tests are performed using $\alpha = \hat{\alpha} = 1$, even if it is to remark that the value of such parameters has no impact on the solution, and, as long as formulation (56) is used, $\alpha = \hat{\alpha} = 0$ could have been also chosen.

7.1. Test Problem 1 (TP1)

Let us consider a cube Ω of edge l inscribed in a cylinder of radius $\hat{R} = \frac{l\sqrt{2}}{2}$ centered in the axis origin and with axis $x = y = 0$, and a cylinder Σ of radius $\check{R} < \hat{R}$ and height $h = l$ whose centreline Λ lies on the z axis (see Figure 3). Let us denote by $\partial\Omega_l$, $\partial\Omega_+$ and $\partial\Omega_-$ respectively the lateral, the top and the bottom faces of the cube. Given $a, b, c, k_1, k_2 \in \mathbb{R}$, let us consider a problem in the form of (20)-(23), obtained by reducing Σ to its centerline, with $K = \tilde{K} = 1$ and

$$f = -\frac{b}{\sqrt{x^2 + y^2}} - 4a, \qquad \overline{\overline{g}} = 0.$$

The problem is completed with the appropriate boundary condition to have the exact solution given by:

$$u_{ex}(x, y, z) = a(x^2 + y^2) + b\sqrt{x^2 + y^2} + c \qquad \text{in } \Omega \qquad (58)$$

$$\hat{u}_{ex}(x, y, z) = k_1 \qquad \text{on } \Lambda \qquad (59)$$

with

$$a = \frac{k_2 - k_1}{(\hat{R} - \check{R})^2}, \quad b = \frac{-2\check{R}(k_2 - k_1)}{(\hat{R} - \check{R})^2}, \quad c = k_1 + \frac{(k_2 - k_1)\check{R}^2}{(\hat{R} - \check{R})^2}$$

This reduced problem corresponds to an equi-dimensional problem satisfying our modeling assumptions and having a constant solution equal to k_1 inside the cylinder. Further, the flux through the interface is zero, as the solution is C^1 in the whole domain. Results are obtained considering a cube of edge $l = 2$ ($\hat{R} = \sqrt{2}$) and choosing $\check{R} = 0.01$, $k_1 = 0.5$ and $k_2 = 5$. Homogeneous Neumann

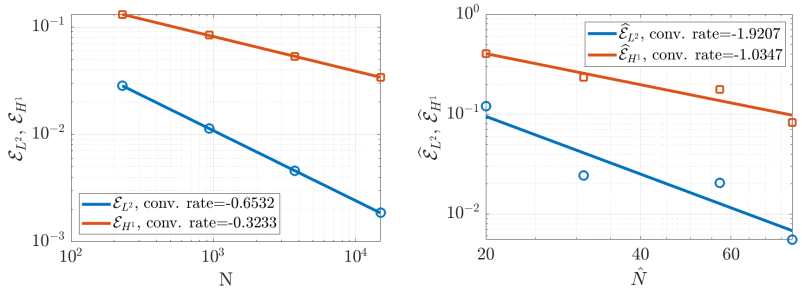

Figure 4: TP1: trend of the L^2 and H^1-norms of the relative errors under mesh refinement. On the left: error committed on the cube with respect to (58); on the right: error committed on the segment with respect to (59). Other parameters: $\hat{\delta}_u = 1$, $\delta_\psi = \delta_\phi = 0.5$.

boundary conditions are imposed on $\partial\Omega_+$ and $\partial\Omega_-$, whereas Dirichlet boundary conditions are imposed on $\partial\Omega_l$. Dirichlet boundary conditions equal to k_1 are imposed on segment endpoints. Figure 3 on the right shows the approximated solutions U, $\hat{U}$ obtained inside the cube and on the segment for $h = 0.086$ and $\hat{\delta}_u = 1$, corresponding to $N = 3715$ DOFs in the cube and $\hat{N} = 57$ DOFs on the segment. The other parameters are $\delta_\phi = 0.5$ and $\delta_\psi = 0.5$. Convergence curves of the error can be computed and, given the regularity of the solution, optimal convergence trends are expected for the used finite element approximation. Let us introduce the errors $\mathcal{E}_{L^2}$, $\mathcal{E}_{H^1}$, for the 3D problem and $\widehat{\mathcal{E}}_{L^2}$ and $\widehat{\mathcal{E}}_{H^1}$ for the 1D problem, defined as follows:

$$\mathcal{E}_{L^2} = \frac{||u_{ex} - U||_{L^2(\Omega)}}{||u_{ex}||_{L^2(\Omega)}}, \qquad \mathcal{E}_{H^1} = \frac{||u_{ex} - U||_{H^1(\Omega)}}{||u_{ex}||_{H^1(\Omega)}},$$
$$\widehat{\mathcal{E}}_{L^2} = \frac{||\hat{u}_{ex} - \hat{U}||_{L^2(\Lambda)}}{||\hat{u}_{ex}||_{L^2(\Lambda)}}, \qquad \widehat{\mathcal{E}}_{H^1} = \frac{||\hat{u}_{ex} - \hat{U}||_{H^1(\Lambda)}}{||\hat{u}_{ex}||_{H^1(\Lambda)}}.$$

Figure 4 displays the convergence trends for the above quantities against mesh refinement. Four meshes are considered, characterized by mesh parameters $h = 0.215, 0.136, 0.086, 0.054$ respectively, corresponding to $N = 229, 933, 3715, 14899$ DOFs and $\hat{N} = 20, 31, 57, 79$ DOFs ($\hat{\delta}_u = 1$, $\delta_\phi = \delta_\psi = 0.5$), confirming the expected behaviors, with a convergence trend close to 0.33 and 0.66 for $\mathcal{E}_{L^2}$ and $\mathcal{E}_{H^1}$, respectively, and of about 2 and 1 for $\widehat{\mathcal{E}}_{L^2}$ and $\widehat{\mathcal{E}}_{H^1}$, respectively. For what concerns the analysis of the behavior of the interface variables Φ and Ψ under mesh refinement let us introduce two further error estimators, i.e.

$$\widehat{\mathcal{E}}_\phi = \sqrt{h}||\phi_{ex} - \Phi||_{L^2(\Lambda)}, \qquad \widehat{\mathcal{E}}_\psi = \frac{||\psi_{ex} - \Psi||_{L^2(\Lambda)}}{||\psi_{ex}||_{L^2(\Lambda)}}.$$

While $\widehat{\mathcal{E}}_\psi$ is in the same form of the error indicators given for the pressure variables, the expression for $\widehat{\mathcal{E}}_\phi$ is chosen to approximate the behavior of a $H^{-\frac{1}{2}}$ norm. According to the considered problem we have $\phi_{ex} = 0$ and $\psi_{ex} = \hat{u}_{ex}$.

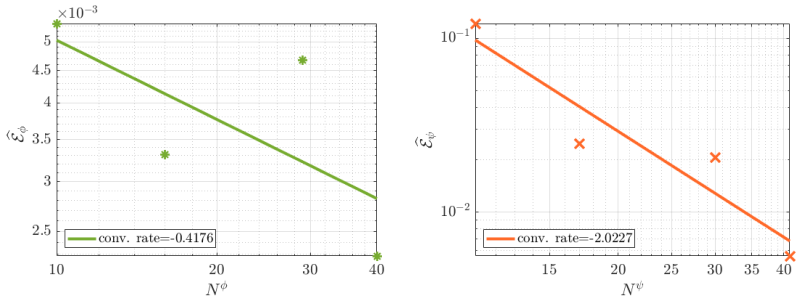

Figure 5: TP1: trend of the error indicators for Φ and Ψ under mesh refinement. On the left $\widehat{\mathcal{E}}_\phi$, on the right $\widehat{\mathcal{E}}_\psi$. Other parameters: $\hat{\delta}_u = 1$, $\delta_\psi = \delta_\phi = 0.5$.

The values of these two error indicators are shown in Figure 5 against mesh refinement: $\widehat{\mathcal{E}}_\phi$ (Figure 5, left) and $\widehat{\mathcal{E}}_\psi$ (Figure 5, right) are plotted against N^ϕ and N^ψ respectively, denoting the number of DOFs for the interface variables ϕ and ψ. We remark that both N^ϕ and N^ψ increase as the 3D mesh is refined since they are linked to the size of the induced mesh through δ_ϕ and δ_ψ. We can observe that $\widehat{\mathcal{E}}_\psi$ shows a convergence behavior very similar to the one of $\widehat{\mathcal{E}}_{L^2}$, as expected. Also the indicator $\widehat{\mathcal{E}}_\phi$ converges to the known solution even if not monotonically and with a rate of about -0.42, due to the fact that we look for a solution in $H^{-\frac{1}{2}}$.

For this simple problem it is possible to compute the condition number of the KKT optimality conditions (55), and analyze how it is affected by different choices of the meshsize of the 1D meshes. Figure 6, on the left, reports the condition number of the KKT system matrix as δ_ϕ varies between 0.1 and 1.5, for values of $\hat{\delta}_u$ between 0.6 and 2, being instead $\delta_\psi = 0.5$ fixed. We can see that δ_ϕ has a relatively small impact on the conditioning of the system as long as $\delta_\phi < \hat{\delta}_u$ is chosen, otherwise a large rapid increase is observed as $\delta_\phi \geq \hat{\delta}_u$ grows. It is therefore advisable to choose a quite coarse mesh for variable Φ with respect to the mesh for $\hat{U}$, even if no theoretical constraints emerged in the analysis. It is however worth highlighting that finer meshes for Φ can be considered, by just increasing the value of $\hat{\delta}_u$. In particular, if $\hat{\delta}_u > 1$, then $\delta_\phi = 1$ becomes a feasible choice with respect to the conditioning. This means that, increasing properly $\hat{\delta}_u$, we can choose a mesh for the flux variable that has the same dimension of the induced mesh, without an excessive growth of the conditioning. Let us observe that this strategy to avoid high condition numbers is not particularly computationally expensive, since only the refinement of a 1D partition, independent from the surrounding 3D mesh, is required. Finally Figure 6, on the right, shows the conditioning of the KKT system matrix as δ_ψ varies between 0.1 and 1.5, keeping this time $\delta_\phi = 0.5$ fixed. It can be seen that, in this case, the conditioning is almost independent of δ_ψ, for all the considered values of $\hat{\delta}_u$.

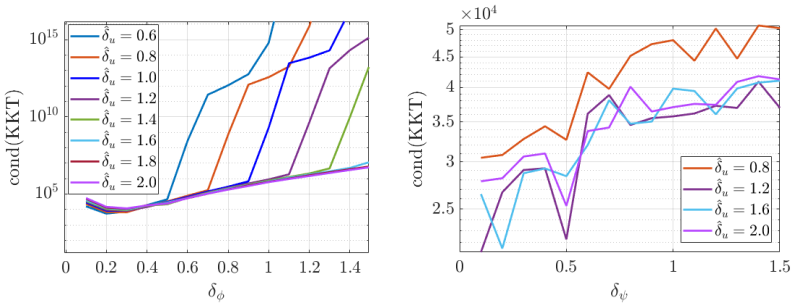

Figure 6: TP1: trend of the conditioning of the KKT system under the variation of the 1D mesh parameters. On the left variable δ_ϕ and different values of $\hat{\delta}_u$, while $\delta_\psi = 0.5$. On the right varibale δ_ψ and $\delta_\phi = 0.5$. In both cases $h = 0.086$.

7.2. Test Problem 2 (TP2)

The second example is set on a domain equal to the one of TP1. We consider three different problems defined as in (20)-(23), characterized by three different values of the coefficient $\tilde{K}$, equal to 1, 10^2 and 10^5 respectively, whereas $K = 1$, $f = 1$, $\overline{\overline{g}} = 0$ are fixed for all the problems. Even the boundary conditions are shared: being $\partial\Omega_+$, $\partial\Omega_-$, and $\partial\Omega_l$ defined as previously, homogeneous Dirichlet boundary conditions are prescribed on $\partial\Omega_+$, $\partial\Omega_-$ and at segment endpoints, while homogeneous Neumann boundary conditions are set on $\partial\Omega_l$.

The accuracy of the solution is evaluated by means of a comparison with an equi-dimensional problem having a cylindrical inclusion of radius 0.01, with centreline coinciding with the 1D domain of the reduced problem. Dirichlet homogeneous boundary conditions are prescribed on the top and bottom faces of the 3D domains and homogeneous Neumann boundary conditions are set on the outer surface. A unitary forcing term is prescribed in the 3D domain outside of the cylindrical inclusion, where, instead a null forcing is set. As $\tilde{K}$ grows, we move from a problem with a smooth solution to a problem with a strong jump of the gradient across the interface between the bulk 3D domain and the inclusion.

The equi-dimensional problem is solved on a fine mesh, refined around the inclusion in order to match the geometry. The lateral surface of the cylindrical inclusion is represented as an extruded regular polygon with 24 edges. The used mesh, along with a detail near the inclusion, is shown in Figure 7, top. As this picture shows, the mesh is strongly refined close to the inclusion, where $h \approx R/5$, locally, in order to correctly catch the geometry and counts about 1.8 million elements and 307299 DOFs.

The reduced 3D-1D problem is solved on four different meshes: first a non conforming mesh, slightly refined close to the inclusion area, is considered, termed adapted mesh and having 2.8×10^4 elements and 4890 DOFs. This mesh has $h \approx R$ close to the inclusion and is thus much coarser than the reference mesh. It is shown in Figure 7, at the bottom, along with a detail of the zone around the 1D domain to highlight the non conformity. Further, three uniformly

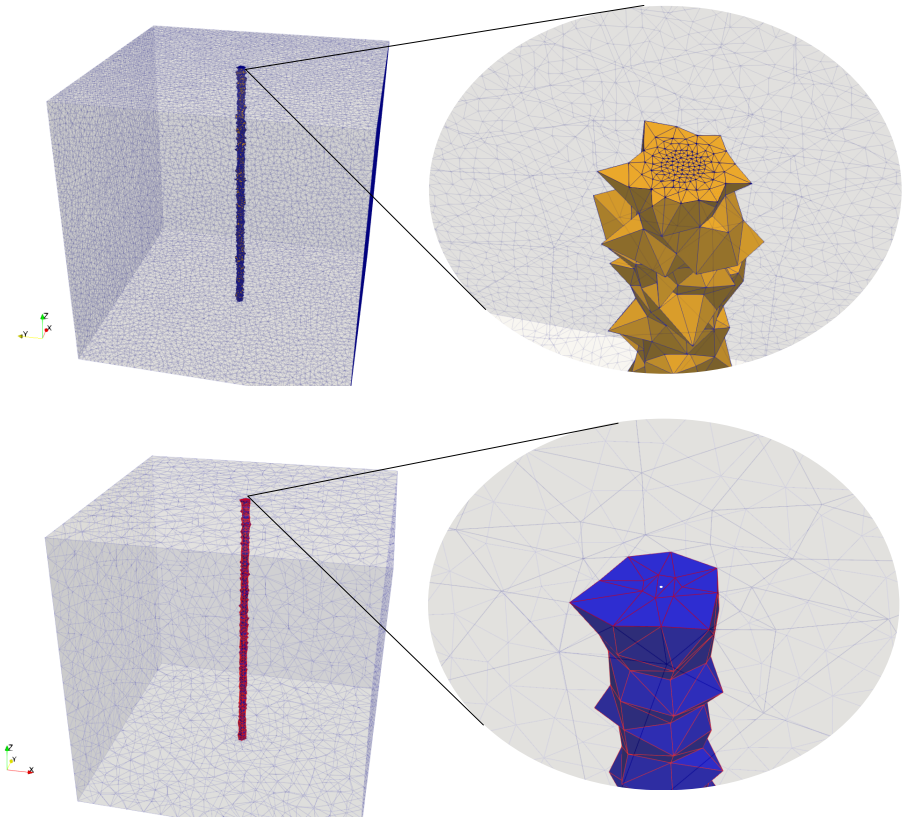

Figure 7: TP2: Top: mesh used for the reference equi-dimensional problem, conforming to the cylindrical inclusion. Bottom: adapted non conforming mesh for the 3D-1D reduced problem with the proposed approach

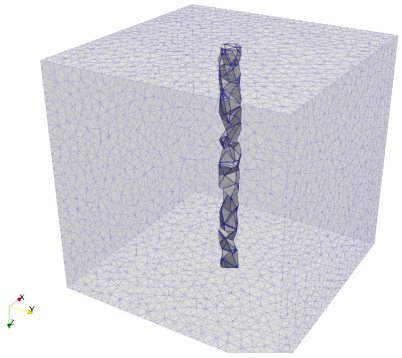

Figure 8: TP2: Uniformly refined mesh with $h = 0.086$.

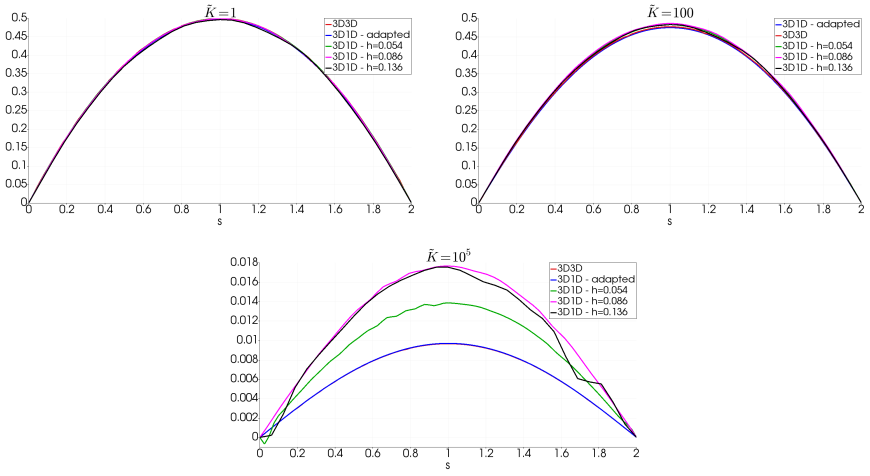

Figure 9: TP2: comparison of the results obtained along the centerline of the cylinder in the 3D-3D conforming setting and by using the 3D-1D reduced model. Other parameters for the 3D-1D setting: $\tilde{\delta}_u = 1$ and $\delta_\phi = \delta_\psi = 0.5$.

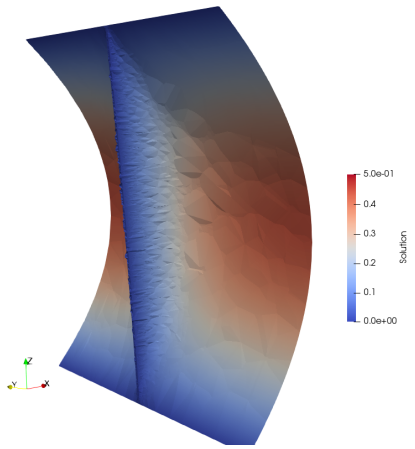

Figure 10: TP2: comparison of the solution obtained on the adapted mesh for the 3D-1D problem with the reference solution on a plane parallel to $y - z$ and containing the centreline of the inclusion. $\tilde{K} = 10^5$.

refined meshes are considered, with mesh parameters $h = 0.136, 0.086, 0.054$, respectively, corresponding to $N = 1287, 4609, 17164$ DOFs. The intermediate uniform mesh is shown in Figure 8.

The solution on the centreline of the inclusion obtained on the various considered meshes are compared to the reference solution on the centreline in Figure 9, for $\tilde{K} = 1$ on the top left, $\tilde{K} = 100$ on the top right, and for $\tilde{K} = 10^5$ on the bottom. We can clearly see that, as long as the jump in the coefficient between the bulk domain and the inclusion is relatively small, the proposed approach correctly reproduces the solution on all the considered meshes. Instead, for large jumps, as it is for $\tilde{K} = 10^5$, the solution on the uniformly refined meshes are less accurate, whereas, the use of a slightly adapted mesh, even if still non conforming, is capable of producing a solution in very good agreement with the reference. This issue is related to the use of a non conforming mesh and is observed also in other works, as e.g. [16, 2], requiring a mesh size of the order of R near the inclusions. The proposed approach can be thus of help in mitigating the overhead in mesh generation and to reduce problem size. A comparison between the reference solution and the solution of the reduced 3D-1D problem on the adapted mesh and with $\tilde{K} = 10^5$ is finally shown in Figure 10, on a slice parallel to the $y - z$ plane and containing the centreline. The plot of the two solutions match well.

7.3. Test with multiple intersecting inclusions (MI)

As for the previous cases, let us consider a cube of edge $l = 2$ centered in the axes origin. Let us then consider a set of 19 inclusions of radius $\check{R} = 10^{-2}$, whose centerlines intersect in 9 points. We impose homogeneous Dirichlet boundary conditions on all the faces of the cube and at the dead ends of the network intersecting cube top and bottom faces, as shown in Figure 11. Homogeneous Neumann boundary conditions are imposed at segment endpoints lying inside the cube. We consider a problem in the same form of (45)-(46), with $i = 1, ..., \mathcal{I} = 19$, spanning the segments, that form a unique connected component, as discussed in Section 6. Further, we consider $K = 1$, $f = 0$ and $\tilde{K}_i = 100$, $\overline{\overline{g}}_i = 100 \ \forall i = 1, ..., 19$.

The problem is solved with both the proposed approach and with a different method, in which the continuity condition $U = \hat{U}$ on all the segments is enforced through the use of Lagrange multipliers, similarly to what suggested in [19] or [8]. We denote this method, used as a comparison, the LM approach, whereas, the three field optimization method is labeled TF. A 3D mesh, non conforming to the inclusions, with $h = 0.056$ and $N = 12873$ and a 1D mesh with $\hat{\delta}_u = 1$, corresponding to $\hat{N} = 309$ DOFs are used for both the methods. Parameters $\delta_\phi = \delta_\psi = 0.5$ are then used for the three field approach, whereas piece-wise constant basis functions are chosen for the Lagrange multipliers for the LM approach, on a 1D mesh of equally spaced-nodes counting one half of the nodes of the mesh for $\hat{U}$.

Figure 11 reports the solutions obtained with the two approaches on the whole network of segments, whereas a comparison of the solutions on two selected segments (as indicated in Figure 11) is reported in Figure 12 on the left,

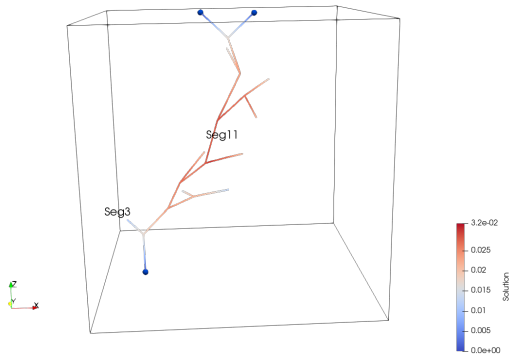

Figure 11: MI: Solution obtained on the centerlines of the inclusions for $h = 0.054$, $\hat{\delta}_u = 1$ and $\delta_\phi = \delta_\psi = 0.5$. Homogeneous Dirichlet boundary conditions are imposed at the points marked in blue.

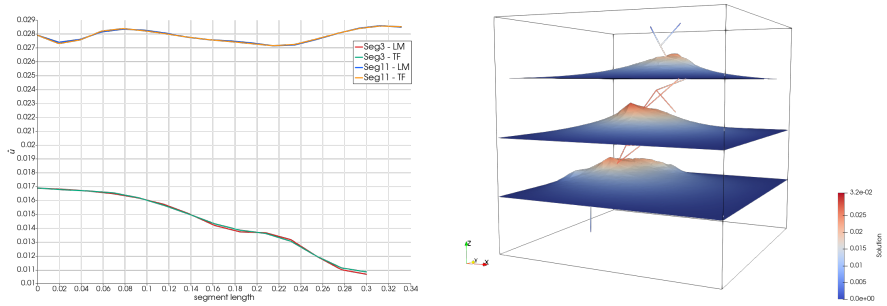

Figure 12: MI: On the left: comparison of the solution on two selected segments with the TF and the LM methods; On the right: solutions with TF and LM obtained inside the cube on three different planes parallel to the $x - y$ plane and located at $z = -0.5$, $z = 0$ and $z = 0.5$. Solution amplified by a factor 10 with respect to domain size.

showing a very good agreement. In Figure 12 on the right, instead, the solution U obtained inside the cube is shown on three different planes, all parallel to the $x - y$ plane and located at $z = -0.5$, $z = 0$ and $z = 0.5$. The solutions with the LM and TF methods are both reported and almost perfectly overlapped, even if the solution is amplified by a factor 10, with respect to domain size in this picture.

Figure 13 displays the behavior of the vector field $-K\nabla U$, obtained with the proposed three field approach.

A quantitative evaluation of the numerical solution provided by the proposed method is provided through an error indicator, denoted by $\Delta_u^{L^2}$, measuring how well the continuity condition, enforced through the minimization of the

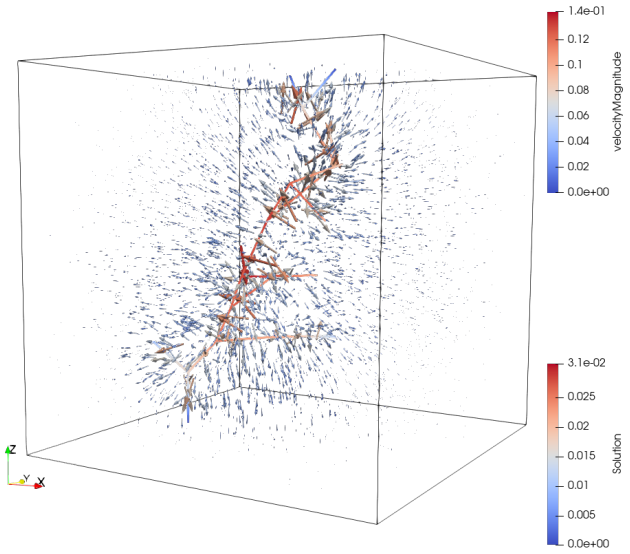

Figure 13: MI: Behavior of the $-K\nabla U$ vector field. The chosen mesh parameters are $h = 0.054$, $\hat{\delta}_u = 1$, $\delta_\phi = \delta_\psi = 0.5$.

functional (53), is satisfied. We thus introduce the quantity:

$$\Delta_u^{L^2} = \frac{\sqrt{\sum_{i=1}^{\mathcal{I}} ||U_{|\Lambda_i} - \hat{U}_i||^2_{L^2(\Lambda_i)}}}{|\max(U, \hat{U})|\sqrt{l_{tot}}} \tag{60}$$

resulting in a non dimensional number, with l_{tot} denoting the total length of the segments in the domain.

The trend of $\Delta_u^{L^2}$ against δ_ϕ and δ_ψ, both ranging between 0.1 and 1, is shown in Figure 14 on the left, still considering $h = 0.054$ and $\hat{\delta}_u = 1$. As expected, the error indicator decreases as the two parameters increase. The impact of δ_ϕ appears to be stronger: for values of δ_ψ close to 1, almost two orders of magnitude are swept by $\Delta_u^{L^2}$ as δ_ϕ varies. The impact of δ_ψ on the continuity condition appears to be weaker, even if it can be seen that it becomes more relevant for high values of δ_ϕ, with almost one order of magnitude swept by the error indicator as δ_ψ increases. Figure 14, on the right, shows instead the trend of $\Delta_u^{L^2}$ against $\hat{\delta}_u$, ranging between 0.6 and 2, for four values of the mesh size h, namely $h = 0.215, 0.136, 0.086, 0.054$, corresponding to $N = 126, 646, 2951, 12873$. The other parameters are $\delta_\phi = \delta_\psi = 0.5$. We can see that the continuity error indicator is only marginally affected by the value of $\hat{\delta}_u$, whereas, it can be arbitrarily reduced by mesh refinement. It should be noted, however, that, for a fixed value of $\hat{\delta}_u$, a refinement of the 3D mesh also implies a refinement of the 1D mesh for $\hat{u}$, whereas, changes in $\hat{\delta}_u$, at fixed h only refine the mesh of $\hat{u}$, leaving the 3D mesh unchanged.

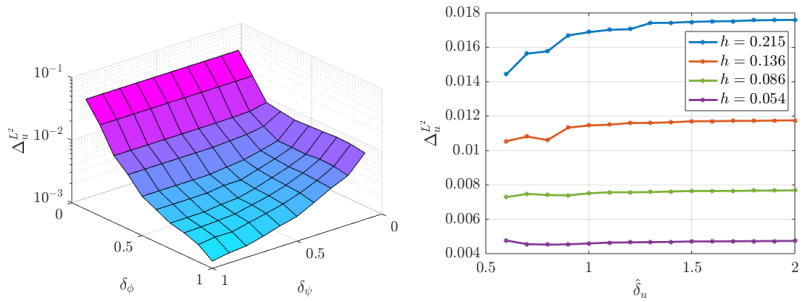

Figure 14: MI: Value of $\Delta_u^{L^2}$ (60) under the variation of the mesh parameters. On the left variable δ_ϕ and δ_ψ, $h = 0.054$; on the right, variable $\hat{\delta}_u$ and four different values of h, $\delta_\phi = \delta_\psi = 0.5$.

8. Conclusions

A novel approach for 3D-1D coupled problems has been proposed. The method derives from a mathematical formulation in proper functional spaces that allows the definition of a well posed trace operator from functions in the three dimensional space to one dimensional manifolds. The 1D problems are decoupled from the problem on the bulk 3D domain and two interface variables are introduced in this domain decomposition process, thus resulting in a three field formulation of the original problem. A cost functional is introduced and minimized to impose matching conditions at the interfaces. The method allows to enforce continuity conditions and flux balance at the interfaces between sub-problems on non-conforming meshes, thus strongly alleviating the mesh generation process. Indeed meshes on the various sub-domains can be independently generated. Numerical results on two simple test problem and on a more complex configuration show the viability of the proposed approach and are used to analyze the effect of method parameters on the condition number of the discrete problem and on solution accuracy.

A formulation suitable for efficient resolution through iterative gradient-based schemes is also envisaged and should be further investigated to allow simulation on problems of high geometrical complexity.

Acknowledgements

This work is supported by the MIUR project "Dipartimenti di Eccellenza 2018-2022" (CUP E11G18000350001), PRIN project "Virtual Element Methods: Analysis and Applications" (201744KLJL_004) and by INdAM-GNCS. Computational resources are partially supported by SmartData@polito.

Appendix

We report in the following Appendix the proof of Proposition 1 and 2, whose statement was provided in Section 4.

Proof of Proposition 1

Proof. Let us compute the Frechet derivatives of the functional with respect to the control variables $\overline{\phi}$ and $\hat{\psi}$. To this end, we introduce increments $\delta\overline{\phi} \in \hat{V}'$ of $\overline{\phi}$ and $\delta\hat{\psi} \in \hat{V}$ of $\hat{\psi}$ and we recall that $\exists\ \delta\psi \in \mathcal{H}^{\Gamma}\ :\ \delta\psi = \mathcal{E}_{\Gamma}\delta\hat{\psi}$. We have:

$$\begin{aligned}
&\frac{\partial J}{\partial\overline{\phi}}(\overline{\phi}+\delta\overline{\phi},\hat{\psi}) = \Big(\gamma_{\Gamma}u(\overline{\phi},\hat{\psi})-\psi,\gamma_{\Gamma}u(\delta\overline{\phi},0)\Big)_{\mathcal{H}^{\Gamma}} + \Big(\gamma_{\Gamma}\tilde{u}(\overline{\phi},\hat{\psi})-\psi,\gamma_{\Gamma}\tilde{u}(\delta\overline{\phi},0)\Big)_{\mathcal{H}^{\Gamma}} = \\
&= \Big(\gamma_{\Gamma}u(\overline{\phi},\hat{\psi})-\mathcal{E}_{\Gamma}\hat{\psi},\gamma_{\Gamma}u(\delta\overline{\phi},0)\Big)_{\mathcal{H}^{\Gamma}} + \Big(\gamma_{\Gamma}\mathcal{E}_{\Sigma}\hat{u}(\overline{\phi},\hat{\psi})-\mathcal{E}_{\Gamma}\hat{\psi},\gamma_{\Gamma}\mathcal{E}_{\Sigma}\hat{u}(\delta\overline{\phi},0)\Big)_{\mathcal{H}^{\Gamma}} = \\
&= \Big\langle\gamma_{\Gamma}^{*}\Theta_{\mathcal{H}^{\Gamma}}(\gamma_{\Gamma}u(\overline{\phi},\hat{\psi})-\mathcal{E}_{\Gamma}\hat{\psi}),u(\delta\overline{\phi},0)\Big\rangle_{V_D',V_D} + \Big\langle{\mathcal{E}_{\Gamma}}^{*}\Theta_{\mathcal{H}^{\Gamma}}(\mathcal{E}_{\Gamma}\hat{u}(\overline{\phi},\hat{\psi})-\mathcal{E}_{\Gamma}\hat{\psi}),\hat{u}(\delta\overline{\phi},0)\Big\rangle_{\hat{V}',\hat{V}} = \\
&= \big\langle A^{*}p,A^{-1}B\delta\overline{\phi}\big\rangle_{V_D',V_D} - \Big\langle\widehat{A}^{*}\hat{p},\widehat{A}^{-1}\widehat{B}\delta\overline{\phi}\Big\rangle_{\hat{V}',\hat{V}} = \\
&= \big\langle B^{*}p,\delta\overline{\phi}\big\rangle_{\hat{V},\hat{V}'} - \Big\langle\widehat{B}^{*}\hat{p},\delta\overline{\phi}\Big\rangle_{\hat{V},\hat{V}'} = \Big(\Theta_{\hat{V}}(B^{*}p-\widehat{B}^{*}\hat{p}),\delta\overline{\phi}\Big)_{\Lambda};
\end{aligned}$$

$$\begin{aligned}
&\frac{\partial J}{\partial\hat{\psi}}(\overline{\phi},\hat{\psi}+\delta\hat{\psi}) = \Big(\gamma_{\Gamma}u(\overline{\phi},\hat{\psi})-\psi,\gamma_{\Gamma}u(0,\delta\hat{\psi})-\delta\psi\Big)_{\mathcal{H}^{\Gamma}} + \Big(\gamma_{\Gamma}\tilde{u}(\overline{\phi},\hat{\psi})-\psi,\gamma_{\Gamma}\tilde{u}(0,\delta\hat{\psi})-\delta\psi\Big)_{\mathcal{H}^{\Gamma}} = \\
&\quad= \Big(\gamma_{\Gamma}u(\overline{\phi},\hat{\psi})-\mathcal{E}_{\Gamma}\hat{\psi},\gamma_{\Gamma}u(0,\delta\hat{\psi})\Big)_{\mathcal{H}^{\Gamma}} - \Big(\gamma_{\Gamma}u(\overline{\phi},\hat{\psi})-\mathcal{E}_{\Gamma}\hat{\psi},\mathcal{E}_{\Gamma}\delta\hat{\psi}\Big)_{\mathcal{H}^{\Gamma}} + \\
&\qquad+ \Big(\gamma_{\Gamma}\mathcal{E}_{\Sigma}\hat{u}(\overline{\phi},\hat{\psi})-\mathcal{E}_{\Gamma}\hat{\psi},\gamma_{\Gamma}\mathcal{E}_{\Sigma}\hat{u}(0,\delta\hat{\psi})\Big)_{\mathcal{H}^{\Gamma}} - \Big(\gamma_{\Gamma}\mathcal{E}_{\Sigma}\hat{u}(\overline{\phi},\hat{\psi})-\mathcal{E}_{\Gamma}\hat{\psi},\mathcal{E}_{\Gamma}\delta\hat{\psi}\Big)_{\mathcal{H}^{\Gamma}} = \\
&\quad= \Big\langle A^{*}p,A^{-1}C\delta\hat{\psi}\Big\rangle_{V_D',V_D} - \Big\langle{\mathcal{E}_{\Gamma}}^{*}\Theta_{\mathcal{H}^{\Gamma}}(\gamma_{\Gamma}u(\overline{\phi},\hat{\psi})-\mathcal{E}_{\Gamma}\hat{\psi}),\delta\hat{\psi}\Big\rangle_{\hat{V}',\hat{V}} + \\
&\qquad+ \Big\langle\widehat{A}^{*}\hat{p},\widehat{A}^{-1}\widehat{C}\delta\hat{\psi}\Big\rangle_{\hat{V}',\hat{V}} - \Big\langle{\mathcal{E}_{\Gamma}}^{*}\Theta_{\mathcal{H}^{\Gamma}}(\mathcal{E}_{\Gamma}\hat{u}(\overline{\phi},\hat{\psi})-\mathcal{E}_{\Gamma}\hat{\psi}),\delta\hat{\psi}\Big\rangle_{\hat{V}',\hat{V}} = \\
&\quad= \Big\langle C^{*}p,\delta\hat{\psi}\Big\rangle_{\hat{V}',\hat{V}} - \Big\langle{\mathcal{E}_{\Gamma}}^{*}\Theta_{\mathcal{H}^{\Gamma}}(\gamma_{\Gamma}u(\delta\overline{\phi},\hat{\psi})-\mathcal{E}_{\Gamma}\hat{\psi}),\delta\hat{\psi}\Big\rangle_{\hat{V}',\hat{V}} + \\
&\qquad\quad+ \Big\langle\widehat{C}^{*}\hat{p},\delta\hat{\psi}\Big\rangle_{\hat{V}',\hat{V}} - \Big\langle{\mathcal{E}_{\Gamma}}^{*}\Theta_{\mathcal{H}^{\Gamma}}(\mathcal{E}_{\Gamma}\hat{u}(\overline{\phi},\hat{\psi})-\mathcal{E}_{\Gamma}\hat{\psi}),\delta\hat{\psi}\Big\rangle_{\hat{V}',\hat{V}} = \\
&\quad= \Big(\Theta_{\hat{V}}^{-1}(C^{*}p+\widehat{C}^{*}\hat{p}-{\mathcal{E}_{\Gamma}}^{*}\Theta_{\mathcal{H}^{\Gamma}}\gamma_{\Gamma}u(\overline{\phi},\hat{\psi})-{\mathcal{E}_{\Gamma}}^{*}\Theta_{\mathcal{H}^{\Gamma}}\mathcal{E}_{\Gamma}\hat{u}(\overline{\phi},\hat{\psi})+2{\mathcal{E}_{\Gamma}}^{*}\Theta_{\mathcal{H}^{\Gamma}}\mathcal{E}_{\Gamma}\hat{\psi}),\delta\hat{\psi}\Big)_{\Lambda},
\end{aligned}$$

which yield the thesis. □

8.1. Proof of Proposition 2

Proof. It is sufficient to set to zero the derivative $\frac{\partial J(\chi+\zeta\delta\chi)}{\partial\zeta}$. In order to get a lighter notation let us set

$$u = u(\overline{\phi},\hat{\psi});\quad \delta u = u(\delta\overline{\phi},\delta\hat{\psi});\qquad \hat{u} = \hat{u}(\overline{\phi},\hat{\psi});\quad \delta\hat{u} = \hat{u}(\delta\overline{\phi},\delta\hat{\psi});$$

$$J(\chi+\zeta\delta\chi)=J(\overline{\phi}+\zeta\delta\overline{\phi},\hat{\psi}+\zeta\delta\hat{\psi})=$$

$$\begin{aligned}
&=\frac{1}{2}\Big(\gamma_\Gamma u(\overline{\phi}+\zeta\delta\overline{\phi},\hat{\psi}+\zeta\delta\hat{\psi})-\psi-\zeta\delta\psi,\gamma_\Gamma u(\overline{\phi}+\zeta\delta\overline{\phi},\hat{\psi}+\zeta\delta\hat{\psi})-\psi-\zeta\delta\psi\Big)_{\mathcal{H}^\Gamma}\\
&+\frac{1}{2}\Big(\gamma_\Gamma \tilde{u}(\overline{\phi}+\zeta\delta\overline{\phi},\hat{\psi}+\zeta\delta\hat{\psi})-\psi-\zeta\delta\psi,\gamma_\Gamma \tilde{u}(\overline{\phi}+\zeta\delta\overline{\phi},\hat{\psi}+\zeta\delta\hat{\psi})-\psi-\zeta\delta\psi\Big)_{\mathcal{H}^\Gamma}=\\
&=\frac{1}{2}\Big(\gamma_\Gamma u+\zeta\gamma_\Gamma\delta u-\mathcal{E}_\Gamma\hat{\psi}-\zeta\mathcal{E}_\Gamma\delta\hat{\psi},\gamma_\Gamma u+\zeta\gamma_\Gamma\delta u-\mathcal{E}_\Gamma\hat{\psi}-\zeta\mathcal{E}_\Gamma\delta\hat{\psi}\Big)_{\mathcal{H}^\Gamma}+\\
&+\frac{1}{2}\Big(\gamma_\Gamma\mathcal{E}_\Sigma\hat{u}+\zeta\gamma_\Gamma\mathcal{E}_\Sigma\delta\hat{u}-\mathcal{E}_\Gamma\hat{\psi}-\zeta\mathcal{E}_\Gamma\delta\hat{\psi},\gamma_\Gamma\mathcal{E}_\Gamma\hat{u}+\zeta\gamma_\Gamma\mathcal{E}_\Gamma\delta\hat{u}-\mathcal{E}_\Gamma\hat{\psi}-\zeta\mathcal{E}_\Gamma\delta\hat{\psi}\Big)_{\mathcal{H}^\Gamma}=\\
&=J(\overline{\phi},\hat{\psi})+\zeta\left(\gamma_\Gamma u-\mathcal{E}_\Gamma\hat{\psi},\gamma_\Gamma\delta u-\mathcal{E}_\Gamma\delta\hat{\psi}\right)_{\mathcal{H}^\Gamma}+\zeta\left(\mathcal{E}_\Gamma\hat{u}-\mathcal{E}_\Gamma\hat{\psi},\mathcal{E}_\Gamma\delta\hat{u}-\mathcal{E}_\Gamma\delta\hat{\psi}\right)_{\mathcal{H}^\Gamma}+\\
&+\frac{\zeta^2}{2}\Big(\gamma_\Gamma\delta u-\mathcal{E}_\Gamma\delta\hat{\psi},\gamma_\Gamma\delta u-\mathcal{E}_\Gamma\delta\hat{\psi}\Big)_{\mathcal{H}^\Gamma}+\frac{\zeta^2}{2}\Big(\mathcal{E}_\Gamma\delta\hat{u}-\mathcal{E}_\Gamma\delta\hat{\psi},\mathcal{E}_\Gamma\delta\hat{u}-\mathcal{E}_\Gamma\delta\hat{\psi}\Big)_{\mathcal{H}^\Gamma}
\end{aligned}$$

$$\begin{aligned}
\frac{\partial J(\chi+\zeta\delta\chi)}{\partial\zeta}&=\left(\gamma_\Gamma u-\mathcal{E}_\Gamma\hat{\psi},\gamma_\Gamma\delta u-\mathcal{E}_\Gamma\delta\hat{\psi}\right)_{\mathcal{H}^\Gamma}+\left(\mathcal{E}_\Gamma\hat{u}-\mathcal{E}_\Gamma\hat{\psi},\mathcal{E}_\Gamma\delta\hat{u}-\mathcal{E}_\Gamma\delta\hat{\psi}\right)_{\mathcal{H}^\Gamma}+\\
&+\zeta\left(\gamma_\Gamma\delta u-\mathcal{E}_\Gamma\delta\hat{\psi},\gamma_\Gamma\delta u-\mathcal{E}_\Gamma\delta\hat{\psi}\right)_{\mathcal{H}^\Gamma}+\zeta\left(\mathcal{E}_\Gamma\delta\hat{u}-\mathcal{E}_\Gamma\delta\hat{\psi},\mathcal{E}_\Gamma\delta\hat{u}-\mathcal{E}_\Gamma\delta\hat{\psi}\right)_{\mathcal{H}^\Gamma}=0
\end{aligned}$$

$$\Rightarrow\ \zeta=-\frac{\left(\gamma_\Gamma u-\mathcal{E}_\Gamma\hat{\psi},\gamma_\Gamma\delta u-\mathcal{E}_\Gamma\delta\hat{\psi}\right)_{\mathcal{H}^\Gamma}+\left(\mathcal{E}_\Gamma\hat{u}-\mathcal{E}_\Gamma\hat{\psi},\mathcal{E}_\Gamma\delta\hat{u}-\mathcal{E}_\Gamma\delta\hat{\psi}\right)_{\mathcal{H}^\Gamma}}{\left(\gamma_\Gamma\delta u-\mathcal{E}_\Gamma\delta\hat{\psi},\gamma_\Gamma\delta u-\mathcal{E}_\Gamma\delta\hat{\psi}\right)_{\mathcal{H}^\Gamma}+\left(\mathcal{E}_\Gamma\delta\hat{u}-\mathcal{E}_\Gamma\delta\hat{\psi},\mathcal{E}_\Gamma\delta\hat{u}-\mathcal{E}_\Gamma\delta\hat{\psi}\right)_{\mathcal{H}^\Gamma}}$$

Rearranging properly the terms we get

$$\zeta=-\frac{\left\langle A^*p,A^{-1}(B\delta\overline{\phi}+C\delta\hat{\psi})\right\rangle_{V_D',V_D}+\left\langle\widehat{A}^*\hat{p},\widehat{A}^{-1}(-\widehat{B}\delta\overline{\phi}+\widehat{C}\delta\hat{\psi})\right\rangle_{\hat{V}',\hat{V}}-\left\langle{\mathcal{E}_\Gamma}^*\Theta_{\mathcal{H}^\Gamma}(\gamma_\Gamma u+\mathcal{E}_\Gamma\hat{u}-2\mathcal{E}_\Gamma\hat{\psi}),\delta\hat{\psi}\right\rangle_{\hat{V}',\hat{V}}}{\left\langle A^{-1}(B\delta\overline{\phi}+C\delta\hat{\psi}),A^*\delta p\right\rangle_{V_D',V_D}+\left\langle\widehat{A}^{-1}(-\widehat{B}\delta\overline{\phi}+\widehat{C}\delta\hat{\psi}),\widehat{A}^*\delta\hat{p}\right\rangle_{\hat{V},\hat{V}'}-\left\langle{\mathcal{E}_\Gamma}^*\Theta_{\mathcal{H}^\Gamma}(\gamma_\Gamma\delta u+\mathcal{E}_\Gamma\delta\hat{u}-2\mathcal{E}_\Gamma\delta\hat{\psi},\delta\hat{\psi})\right\rangle_{\hat{V}',\hat{V}}}=$$

$$=-\frac{\left\langle B^*p,\delta\overline{\phi}\right\rangle_{\hat{V},\hat{V}'}+\left\langle C^*p,\delta\hat{\psi}\right\rangle_{\hat{V}',\hat{V}}-\left\langle\widehat{B}^*\hat{p},\delta\overline{\phi}\right\rangle_{\hat{V},\hat{V}'}+\left\langle\widehat{C}^*\hat{p},\delta\hat{\psi}\right\rangle_{\hat{V}',\hat{V}}-\left\langle{\mathcal{E}_\Gamma}^*\Theta_{\mathcal{H}^\Gamma}(\gamma_\Gamma u+\mathcal{E}_\Gamma\hat{u}-2\mathcal{E}_\Gamma\hat{\psi}),\delta\hat{\psi}\right\rangle_{\hat{V}',\hat{V}}}{\left\langle B\delta\overline{\phi}+C\delta\hat{\psi},\delta p\right\rangle_{V_D',V_D}+\left\langle-\widehat{B}\delta\overline{\phi}+\widehat{C}\delta\hat{\psi},\delta\hat{p}\right\rangle_{\hat{V}',\hat{V}}-\left\langle{\mathcal{E}_\Gamma}^*\Theta_{\mathcal{H}^\Gamma}(\gamma_\Gamma\delta u+\mathcal{E}_\Gamma\delta\hat{u}-2\mathcal{E}_\Gamma\delta\hat{\psi}),\delta\hat{\psi}\right\rangle_{\hat{V}',\hat{V}}}=$$

$$=-\frac{\left(\delta\overline{\phi},\delta\overline{\phi}\right)_\Lambda+\left(\delta\hat{\psi},\delta\hat{\psi}\right)_\Lambda}{\left\langle B\delta\overline{\phi}+C\delta\hat{\psi},\delta p\right\rangle_{V_D',V_D}+\left\langle-\widehat{B}\delta\overline{\phi}+\widehat{C}\delta\hat{\psi},\delta\hat{p}\right\rangle_{\hat{V}',\hat{V}}-\left\langle{\mathcal{E}_\Gamma}^*\Theta_{\mathcal{H}^\Gamma}(\gamma_\Gamma\delta u+\mathcal{E}_\Gamma\delta\hat{u}-2\mathcal{E}_\Gamma\delta\hat{\psi}),\delta\hat{\psi}\right\rangle_{\hat{V}',\hat{V}}}$$

that yields the thesis. □

References

[1] D. Notaro, L. Cattaneo, L. Formaggia, A. Scotti, P. Zunino, A Mixed Finite Element Method for Modeling the Fluid Exchange Between Microcirculation and Tissue Interstitium, Springer International Publishing, 2016, pp. 3–25. doi:10.1007/978-3-319-41246-7_1.

[2] T. Köppl, E. Vidotto, B. Wohlmuth, A 3d-1d coupled blood flow and oxygen transport model to generate microvascular networks, International Journal for Numerical Methods in Biomedical Engineering 36 (10) (2020) e3386. doi:10.1002/cnm.3386.

[3] N. Schröder, M. Javaux, J. Vanderborght, B. Steffen, H. Vereecken, Effect of root water and solute uptake on apparent soil dispersivity: A simulation study, Vadose Zone Journal 11 (3) (2012) vzj2012.0009. doi:https://doi.org/10.2136/vzj2012.0009.

[4] T. Koch, K. Heck, N. Schröder, H. Class, R. Helmig, A new simulation framework for soil–root interaction, evaporation, root growth, and solute transport, Vadose Zone Journal 17 (1) (2018) 170210. doi:10.2136/vzj2017.12.0210.

[5] I. G. Gjerde, K. Kumar, J. M. Nordbotten, Well modelling by means of coupled 1d-3d flow models, in: ECMOR XVI - 16th European Conference on the Mathematics of Oil Recovery, 2018.

[6] I. Gjerde, K. Kumar, J. Nordbotten, A singularity removal method for coupled 1d–3d flow models, Comput Geosci 24 (2020) 443–457. doi:10.1007/s10596-019-09899-4.

[7] D. Cerroni, F. Laurino, P. Zunino, Mathematical analysis, finite element approximation and numerical solvers for the interaction of 3d reservoirs with 1d wells, GEM - International Journal on Geomathematics 10 (1).

[8] I. Steinbrecher, M. Mayr, M. Grill, J. Kremheller, C. Meier, A. Popp, A mortar-type finite element approach for embedding 1d beams into 3d solid volumes, Comput Mech 66 (2020) 1377–1398. doi:10.1007/s00466-020-01907-0.

[9] A. Llau, L. Jason, F. Dufour, J. Baroth, Finite element modelling of 1d steel components in reinforced and prestressed concrete structures, Engineering Structures 127 (2016) 769–783. doi:10.1016/j.engstruct.2016.09.023.

[10] C. D'Angelo, Finite element approximation of elliptic problems with dirac measure terms in weighted spaces: applications to one- and three-dimensional coupled problems, SIAM J. Numer. Anal. 50 (1) (2012) 194 – 215.

[11] C. D'Angelo, A. Quarteroni, On the coupling of 1d and 3d diffusion-reaction equations. application to tissue perfusion problems, Math. Models Methods Appl. Sci. 18 (2008) 1481 – 1504.

[12] A. Ern, J. Guermond, Theory and Practice of Finite Elements, Vol. 159, Appl. Mat. Sci, Springer-Verlag, New York, 2004.

[13] A.-K. Tornberg, B. Engquist, Numerical approximations of singular source terms in differential equations, Journal of Computational Physics 200 (2) (2004) 462–488. doi:10.1016/j.jcp.2004.04.011.

[14] Gjerde, Ingeborg G., Kumar, Kundan, Nordbotten, Jan M., Wohlmuth, Barbara, Splitting method for elliptic equations with line sources, ESAIM: M2AN 53 (5) (2019) 1715–1739. doi:10.1051/m2an/2019027.

[15] T. Köppl, E. Vidotto, B. Wohlmuth, P. Zunino, Mathematical modeling, analysis and numerical approximation of second-order elliptic problems with inclusions, Mathematical Models and Methods in Applied Sciences 28 (05) (2018) 953–978. doi:10.1142/S0218202518500252.

[16] L. Heltai, A. Caiazzo, Multiscale modeling of vascularized tissues via non-matching immersed methods, International Journal for Numerical Methods in Biomedical Engineering 35 (12) (2019) e3264. doi:10.1002/cnm.3264.

[17] T. Koch, M. Schneider, R. Helmig, P. Jenny, Modeling tissue perfusion in terms of 1d-3d embedded mixed-dimension coupled problems with distributed sources, Journal of Computational Physics 410 (2020) 109370. doi:10.1016/j.jcp.2020.109370.

[18] F. Laurino, P. Zunino, Derivation and analysis of coupled pdes on manifolds with high dimensionality gap arising from topological model reduction., ESAIM: M2AN 53 (6) (2019) 2047 – 2080.

[19] M. Kuchta, F. Laurino, K.-A. Mardal, P. Zunino, Analysis and approximation of mixed-dimensional pdes on 3d-1d domains coupled with lagrange multipliers, SIAM Journal on Numerical Analysis 59 (1) (2021) 558–582. doi:10.1137/20M1329664.

[20] F. Brezzi, L. Marini, A three-field domain decomposition method, Contemporary Mathematics 157.

[21] S. Berrone, D. Grappein, S. Pieraccini, S.Scialò, A three-field based optimization formulation for flow simulations in networks of fractures on non conforming meshes, accepted for publication on SIAM J. Sci. Comput. (2019). arXiv:1912.09744.

[22] C. Giverso, P. Ciarletta, Tumour angiogenesis as a chemo-mechanical surface instability, Sci Rep 6 (2016) 22610. doi:10.1038/srep22610.

[23] M. A. J. Chaplain, C. Giverso, T. Lorenzi, L. Preziosi, Derivation and application of effective interface conditions for continuum mechanical models of cell invasion through thin membranes, SIAM Journal on Applied Mathematics 79 (5) (2019) 2011–2031. doi:10.1137/19M124263X.

[24] S. Berrone, S. Pieraccini, S. Scialò, An optimization approach for large scale simulations of discrete fracture network flows, J. Comput. Phys. 256 (2014) 838–853. doi:10.1016/j.jcp.2013.09.028.

[25] S. Berrone, S. Scialò, F. Vicini, Parallel meshing, discretization and computation of flow in massive Discrete Fracture Networks, SIAM J. Sci. Comput. 41 (4) (2019) C317–C338. doi:10.1137/18M1228736.

[26] S. Berrone, A. D'Auria, S. Scialò, An optimization approach for flow simulations in poro-fractured media with complex geometries, Comput Geoscidoi:10.1007/s10596-020-10029-8.

[27] S. Pieraccini, Uncertainty quantification analysis in discrete fracture network flow simulations, Int J Geomath 11. doi:10.1007/s13137-020-0148-0.

[28] C. Canuto, S. Pieraccini, D. Xiu, Uncertainty quantification of discontinuous outputs via a non-intrusive bifidelity strategy, Journal of Computational Physics 398 (2019) 108885. doi:10.1016/j.jcp.2019.108885.

[29] J. Pestana, T. Rees, Null-space preconditioners for saddle point systems, SIAM Journal on Matrix Analysis and Applications 37 (3) (2016) 1103–1128. doi:10.1137/15M1021349.